STABILITY AND MIXING OF SUBMERGED TURBULENT JETS AT LOW REYNOLDS NUMBERS

by

Christopher D. Ungate, Donald R. F. Harleman,
and Gerhard H. Jirka

Energy Laboratory Report Number MIT-EL 75-014

February 1975

STABILITY AND MIXING OF SUBMERGED TURBULENT JETS AT LOW REYNOLDS NUMBERS

by

Christopher D. Ungate

Donald R. F. Harleman

and

Gerhard H. Jirka

ENERGY LABORATORY

in association with

RALPH M. PARSONS LABORATORY

FOR

WATER RESOURCES AND HYDRODYNAMICS

Department of Civil Engineering

MASSACHUSETTS INSTITUTE OF TECHNOLOGY

Sponsored by

New England Electric System and Northeast Utilities Service Company

under the

M.I.T. Energy Laboratory

Electric Power Program

Energy Laboratory Report No. MIT-EL 75-014 February 1975

R. M. Parsons Technical Report No. 197

ABSTRACT

An experimental study is made of the variation of volume and centerline dilution as a function of Reynolds number in non-buoyant and buoyant round jets discharged vertically from a submerged nozzle. The jet Reynolds numbers covered the laminar-turbulent transition with values ranging from $Re = u_o D/\nu = 100$ to 20,000 where u_o = jet exit velocity, D = jet diameter, and ν = kinematic viscosity. Measurements of jet temperature profiles are obtained by using both fast and slow thermistor probes.

Turbulent dilution is found to be independent of Reynolds number for non-buoyant jets above a critical Reynolds number of about 1,500. For buoyant jets (densimetric Froude numbers in the range 25 to 50), the critical Reynolds number is about 1,200. Reasonable agreement is obtained with the results of previous investigators for dilution values at high Reynolds numbers. Dye studies of transition Reynolds numbers are compared with a study by A.F. Pearce (1966) and good agreement is found.

The results are useful in determining the minimum length scale ratio for hydro-thermal model studies, especially those of submerged multiport diffusers. It is concluded that modeling of turbulent jets is acceptable provided the model Reynolds number is larger than the critical Reynolds number and provided no other constraint becomes binding. In addition, the model jet's laminar length, if any, must be insignificant when compared to the total length of the path of the jet.

ACKNOWLEDGEMENTS

Funds for the publication of this report were provided by the research program on once-through cooling systems within the Waste Heat Management Group of the M.I.T. Energy Laboratory (OSP 82070). Funds for computer time for the data reduction program were provided by the M.I.T. Joint Civil Engineering-Mechanical Engineering Computer Facility.

The authors gratefully acknowledge suggestions and comments by Professor Keith D. Stolzenbach. Technical assistance was provided by Mr. Roy Milley, Machinist, and Mr. Edward McCaffrey, electrical engineer. Photographs were printed by Mr. Milan J. Merhar, Jr. Graphs were drawn by Mr. Stanley Mitchell, and the manuscript was typed by Mrs. Stephanie Demeris.

The material contained in this report was submitted by Christopher D. Ungate to the Department of Civil Engineering in partial fulfillment of the requirements for the degree of Master of Science. Research supervision was provided by Donald R.F. Harleman, Professor of Civil Engineering, and Director of the Ralph M. Parsons Laboratory for Water Resources and Hydrodynamics, and Gerhard Jirka, Research Engineer, M.I.T. Energy Laboratory.

TABLE OF CONTENTS

	Page
TITLE PAGE	1
ABSTRACT	2
ACKNOWLEDGEMENTS	3
TABLE OF CONTENTS	4
LIST OF TABLES	6
LIST OF FIGURES	7
I. INTRODUCTION	9
II. STATEMENT OF THE PROBLEM	10
III. PREVIOUS STUDIES	13
IV. ANALYSIS	18
A. Determination of Parameters	18
B. Definition of Dilution	20
C. Results of Previous Investigations	24
D. Temperature as an Indicator of Dilution	29
V. EXPERIMENTAL APPARATUS AND DATA REDUCTION	32
A. Apparatus	32
B. Experimental Procedure	36
C. Data Reduction	38
D. Sources of Error	43
1. Sources of Error in Flow Measurement	43
2. Sources of Error in Temperature Regulation and Measurement	44
3. Sources of Error in Photographs	44
4. General Discussion of Errors	45
VI. RESULTS AND DISCUSSION	47
A. General Presentation of Results	47
B. Non-buoyant Jets	53
C. Buoyant Jets	65

		Page
VII.	CONCLUSIONS	77
	A. Non-buoyant Jets	77
	B. Buoyant Jets	77
VIII.	FUTURE WORK	79
IX.	REFERENCES	81

LIST OF TABLES

		Page
Table 1	Values of Coefficient S^*_v Found for Non-buoyant Axisymmetric Jets	25
Table 2	Values of Coefficient S^*_c Found for Non-buoyant axisymmetric Jets	27
Table 3	Values of Coefficient S^*_c Found for Buoyant Axisymmetric Jets	28
Table 4	Experimental Results for Froude Number = 100	48
Table 5	Experimental Results for Froude Number = 50	49
Table 6	Experimental Results for Froude Number = 25	50
Table 7	Experimental Results for Froude Number = 10	51
Table 8	Laminar Length and Cone Angle for Non-buoyant Jets	58
Table 9	Laminar Length and Cone Angle for Buoyant Jets	70

LIST OF FIGURES

		Page
Figure 1	Examples of Non-buoyant Jets Given by Pearce (18)	14
Figure 2	Submerged, Vertical Axisymmetric Jet	19
Figure 3	Concentration and Velocity along Axis of Three Dimensional Jet (after Abraham (2))	30
Figure 4	Schematic of Experimental Setup	33
Figure 5	Nozzle Assembly	34
Figure 6a	Selection of Best Profile from a Number of Traverses at $z/d_o = 10$	39
Figure 6b	Radial Profile Obtained from Figure 6a	39
Figure 6c	Examples of Temperature Fluctuation, Jet Diameter Definition and Mean Profiles for Various Froude Numbers	40
Figure 6d	Examples of Definition of Diameter	41
Figure 7	Inverse Centerline Dilution versus z/d_o for Non-buoyant and Buoyant Turbulent Jets	52
Figure 8	S_c versus Reynolds Number for Non-buoyant Jets at $z/d_o = 15$	54
Figure 9	S_c^* versus Reynolds Number for Non-buoyant Jets	55
Figure 10	S_V^* versus Reynolds Number for Non-buoyant Jets ($\lambda^2 = 2$)	57
Figure 11	Laminar Length versus Reynolds Number for Non-buoyant Jets	59
Figure 12	Cone Angle versus Reynolds Number for Non-buoyant Jets	60
Figure 13	Examples of Non-buoyant Jets	62

		Page
Figure 14	S_c versus Reynolds Number for Buoyant Jets at $z/d_o = 15$	66
Figure 15	S_c^* versus Reynolds Number for Buoyant Jets	67
Figure 16	$S_\forall^*$ versus Reynolds Number for Buoyant Jets ($\lambda^2 = 2$)	68
Figure 17	Laminar Length versus Reynolds Number for Buoyant Jets	71
Figure 18	Cone Angle versus Reynolds Number for Buoyant Jets	72
Figure 19	Examples of Buoyant Jets	74

I. Introduction

Multiport diffusers are used to discharge heated cooling water from power plants into natural bodies of water in order to satisfy thermal discharge criteria by inducing dilution of the discharge. The use of such diffusers and the application of mathematical prediction models have been discussed by several investigators (10,14). When proposed sites for diffusers have complex topography and non-uniform or unsteady ambient currents, an initial design can be tested or modified by means of a hydraulic scale model. A discussion of modeling requirements must necessarily include the assumptions and tradeoffs of such models, since, in general, all relevant dimensionless parameters cannot be kept equal in model and prototype. For models of thermal discharges, the model and prototype densimetric Froude number, which relates gravity and buoyancy forces, must be identical. Since, in addition, it is common practice to have approximately the same temperature rise in both model and prototype, it is then impossible to equate model and prototype jet Reynolds numbers. This fact not only brings into question the use of models whose jet Reynolds number falls into the laminar-turbulent transition, but also limits the physical size of such models by limiting the length scale ratio. The purpose of this study is to investigate the variation of jet dilution with Reynolds number, particularly in the laminar-turbulent transition of importance in model studies.

II Statement of the Problem

As stated previously, a basic requirement for any thermal discharge problem is the equality of densimetric Froude numbers. The densimetric Froude number is given by:

$$F = \frac{V}{\left(\frac{\Delta\rho}{\rho_1} g L\right)^{1/2}} \tag{1}$$

where V = characteristic velocity

L = characteristic length

ρ_1 = reference density

$\Delta\rho$ = characteristic density difference.

For a submerged jet, the initial densimetric Froude number is calculated using the jet exit velocity, nozzle diameter, ambient density, and the density difference between the ambient water and the jet discharge. Denoting, with the subscript r, the ratio between model and prototype, the velocity ratio is given by:

$$V_r = \sqrt{\left(\frac{\Delta\rho}{\rho_1}\right)_r g_r L_r} \tag{2}$$

Since it is common practice to have approximately the same temperature in the model as in the prototype, the velocity ratio becomes:

$$V_r = \sqrt{L_r} \tag{3}$$

An additional requirement for a jet diffusion model is that the model be large enough to insure turbulent jet entrainment. The jet Reynolds number is given by:

$$Re = \frac{V\,L}{\nu} \tag{4}$$

where ν = kinematic viscosity of the discharge fluid.
For a submerged, axisymmetric jet, the Reynolds number is calculated using the jet exit velocity and the nozzle diameter, and is constant along the entire path of the jet for both the laminar and the turbulent case.

Denoting, again, with the subscript r, the model to prototype ratio, it can be seen that $\nu_r = 1$, since $(\frac{\Delta\rho}{\rho_1})_r = 1$. Thus the ratio of Reynolds numbers becomes, after substituting Equation 3 into Equation 4:

$$Re_r = L_r^{3/2} \tag{5}$$

Thus it can be seen that the minimum size of physical scale models of thermal discharges is limited by the turbulent jet entrainment requirement. A typical prototype jet Reynolds number for a diffuser discharge, such as the Maine Yankee Atomic Power Station (15), is approximately 2.5×10^6. In order to meet the Reynolds criterion just discussed, a length scale ratio equal to or greater than 1/100 was necessary for model studies of the cooling water discharge. If the dilution of a lower Reynolds number jet were

known to be equivalent to that of a fully turbulent jet, a smaller length scale ratio could have been employed for these model studies, provided no other physical constraint would become binding.

The purpose of submerged jets is to dilute their discharge by entraining and mixing ambient fluid through turbulent diffusion. For jets which are in the laminar-turbulent transition range of Reynolds numbers, it is reasonable to expect that this entrainment, and hence the dilution, will decrease because of the lower turbulent intensity of the jets. Pearce (18) has made a qualitative investigation of Reynolds number effects on submerged jets in the laminar-turbulent transition by means of dye studies. He concluded that flow in a submerged circular jet will normally have fully turbulent structure for values of the Reynolds number exceeding 3000. Jets which were in the laminar-turbulent transition could then be considered less efficient in entraining ambient fluid than fully turbulent jets. Model results under such conditions have been judged to be on the conservative side with respect to the dilution capacity of the jets. This study will examine quantitatively the variation of jet dilution with Reynolds number in the laminar-turbulent transition of importance to thermal model studies.

III Previous Studies

Little previous work has been published which studies Reynolds number effects on jet dilution. The most important of these is that of Pearce (18), who made visual observations using dye of the structure of nearly non-buoyant jets over a Reynolds number range of 68 to 13,100. His definition of jet Reynolds number is the same as that mentioned earlier. Each jet was photographed and from each picture the length of any non-turbulent zone, z_1/d_o, and the angle of spread of the turbulent zone, $2\alpha_t^o$, was measured. Pearce defined d_o as the initial jet diameter and α_t^o as the angle of spread of the outer jet boundary from the jet axis. Some examples of his photographs are shown in Figure 1. His results are summarized as follows:

Re < 500	Jet is essentially laminar. Any instabilities are rapidly damped.
500 < Re < 1500	At some distance from the nozzle, the jet becomes unstable and breaks down into turbulent eddies. As the Reynolds number increases, the laminar zone expands less rapidly and decreases in length.
1500 < Re < 2500	The laminar length continues to decrease until it disappears at 2000 < Re < 2500. The angle of spread of the turbulent zone decreases. The turbulent zone breaks

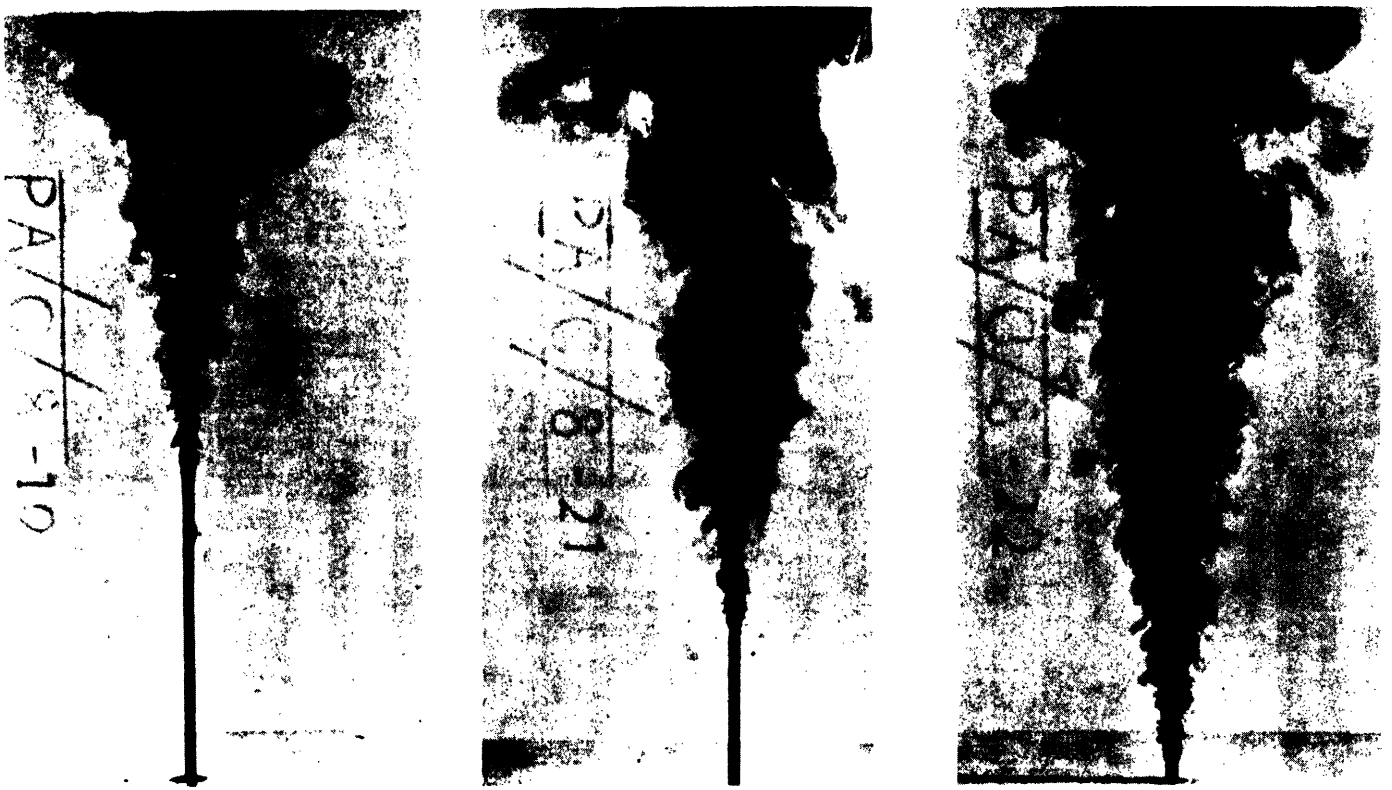

Re = 1020 Re = 1480 Re = 1938

Figure 1. Examples of Non-buoyant jets given by Pearce(18)

	down completely to turbulence.
$2500 < Re < 3000$	The spread of the turbulent zone continues to decrease.
$3000 < Re$	Jet has fully turbulent structure and cone angle is constant.

On this basis, Pearce concluded that a circular jet whose Reynolds number was less than 3000 was not fully turbulent and, therefore, did not have full dilution capability.

Pearce's report cites many other works which discuss the transition from laminar to turbulent flow in circular jets from the point of view of jet structure and stability. Mollendorf and Gebhart (17) have also reviewed this aspect of transition flows, designating two general approaches: that of measuring the laminar length of transition jets and that of introducing small disturbances into the flow and studying jet instability. These studies, while perhaps of importance for theoretical verification, are hampered by the stochastic nature of the phenomena they investigate. After an attempt to answer the jet instability question has been completed, these works still leave untouched the problem of the relative importance of the various phenomena measured, such as laminar length, cone angle or eddy size and structure, to the dilution capability of importance to the engineer. Certainly more efforts are needed to attempt to understand these relationships.

No reports are available in the literature which attempt to directly measure dilution parameters in the full range of transition Reynolds numbers. Albertson, et al (4), performed experimental work on plane and circular isothermal jets. Their results showed no Reynolds number effects on jet dilution in the range of Reynolds numbers studied. The lowest Reynolds number studied was Re = 1500. Ricou and Spalding (19) measured mass entrainment rates over a range of Reynolds numbers and estimated a critical Reynolds number of 25,000 over which the rate of entrainment was constant. Some doubt exists as to whether the experimental method of measuring entrainment used by Ricou and Spalding affects their results. They placed a porous collar around the entrainment region of the jet and measured the entrainment by noting the change in head across the collar. Pearce quotes the work of Baines, who showed Reynolds number effects on the velocity distribution and on the length of the potential core in the zone of flow establishment below a Reynolds number of 200,000. This, Pearce suggests, shows that the flow was not fully developed even in this range.

The wide range of results quoted in this discussion and in those of Pearce, Mollendorf and Gebhart, indicates the difficulty in drawing conclusions concerning dilution capacity of transition jets from experimental evidence which quotes data on structural properties, or which studies effects on jets over an incomplete range of Reynolds numbers, or which quotes data of wide scatter

supporting differing conclusions. This study, by measuring jet dilution, a characteristic parameter of practical importance, attempts to provide evidence of overall behavior which can form a basis for weighting the relative importance of these properties and quantities.

IV Analysis

A. Determination of Parameters

For the case of a vertical, axisymmetric buoyant or non-buoyant jet, shown schematically in Figure 2, issuing into a calm ambient fluid of uniform density, the following variables may be identified:

z = distance measured in the vertical direction along the jet axis

r = distance from the jet axis measured in the radial direction

d = diameter of the jet, defined by the intersection of the temperature profile with the local ambient temperature

d_o = nozzle diameter

u = vertical velocity

ρ = density

T = temperature

ν = kinematic viscosity

subscripts:

o = initial value of variable

c = centerline value of variable

a = ambient reference value

$\Delta T = T - T_a$

$\Delta \rho = \rho - \rho_a$

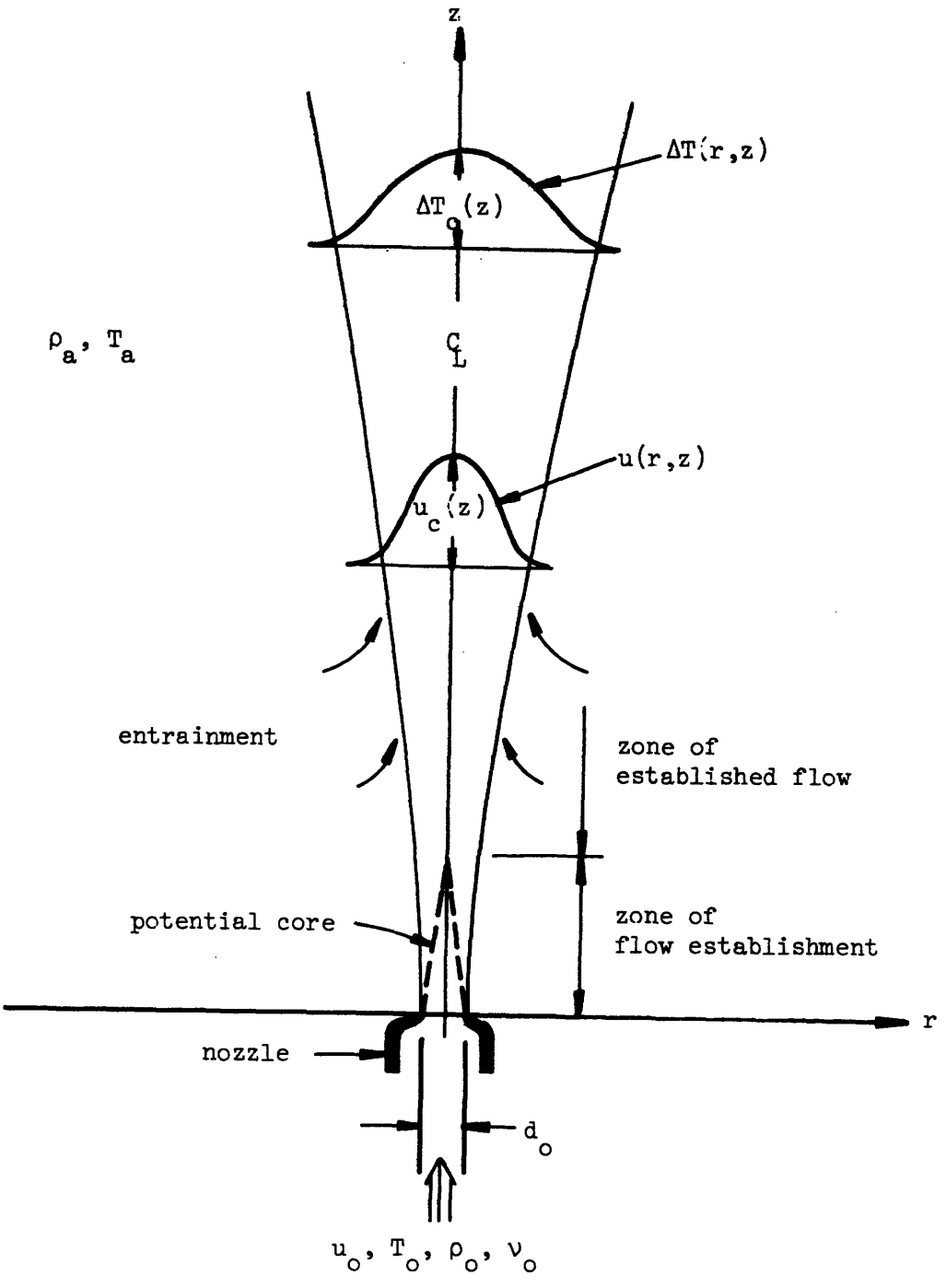

Figure 2. Submerged, Vertical, Axisymmetric Jet

Abraham (1) has shown the results of dimensional analysis for this case to be (with minor changes in definition):

$$\frac{u}{u_o} = f\left(\frac{z}{d_o}, \frac{r}{d_o}, \frac{\Delta\rho}{\rho_a}, F, Re\right) \tag{6}$$

$$\frac{c}{c_o} = f_2\left(\frac{z}{d_o}, \frac{r}{d_o}, \frac{\Delta\rho}{\rho_a}, F, Re\right) \tag{7}$$

where $c = \Delta\rho/\Delta\rho_o$

$c_o = 1$

The densmietric Froude number and the Reynolds number have been defined previously. By making the Boussinesq approximation, density deviations from the ambient density introduced by the jet discharge are small compared to the local density $\rho(r,z)$. By using temperature as an indicator of changes in the concentration c, the previous relationships become:

$$\frac{u}{u_o} = r_1\left(\frac{z}{d_o}, \frac{r}{d_o}, F, Re\right) \tag{8}$$

$$\frac{\Delta T}{\Delta T_o} = f_2\left(\frac{z}{d_o}, \frac{r}{d_o}, F, Re\right) \tag{9}$$

B. Definition of Dilution

A definition of dilution is needed to further simplify the problem. A volume dilution can be defined as:

$$S_V = \frac{Q}{Q_o} = \frac{\int_A u \, dA}{Q_o} \tag{10}$$

where A = crossectional area .

Also, a centerline temperature dilution can be defined as:

$$S_c = \frac{\Delta T_o}{\Delta T_c} \tag{11}$$

Strictly speaking, the centerline dilution is not a dilution, but actually a centerline reduction factor which can be related to the volume dilution by making some assumption about the structure of the jet. Since the literature commonly refers to Equation 11 as centerline dilution, this terminology will also be used here.

Since only temperature has been measured in the jet, only S_c can be directly evaluated. The volume dilution can be derived by making the following assumptions for u and ΔT:

$$\frac{u}{u_c} = f_u\left(\frac{r}{d}\right) \tag{12}$$

$$\frac{\Delta T}{\Delta T_c} = f_T\left(\frac{r}{d}\right) \tag{13}$$

where d = diameter of the jet defined by the intersection of the temperature profile with the local ambient temperature

Assume that the velocity and temperature profiles are related as follows:

$$\frac{u}{u_c} = \left(\frac{\Delta T}{\Delta T_c}\right)^{\lambda^2} \qquad (14)$$

where λ = experimentally determined spreading ratio accounting for dissimilarity of velocity and temperature profiles.

Taylor's theory of free turbulence finds that $\lambda^2 = 2$ for a circular turbulent jet. The value of λ will change as the level of turbulent intensity changes. For sections where the turbulent intensity is low, the spreading of the temperature profile will be smaller than that for a turbulent section; thus, an assumption of a turbulent λ will underestimate the flow at a section of lower turbulent intensity, and give a lower value of dilution.

Substitution of these assumptions for the velocity and temperature profiles into Equation 10 gives:

$$S_V = \frac{u_c}{Q_o} \int_A f_T^{\lambda^2} \, dA \qquad (15)$$

Conservation of heat content is given by:

$$\rho_o c_{po} Q_o \Delta T_o = \int_A \rho c_p u \Delta T \, dA \qquad (16)$$

where c_p = specific heat at constant pressure

To simplify this equation, it is assumed that $\rho_o c_{po} \approx \rho c_p$ = constant. This indicates that the heat content per unit volume and degree temperature change is constant, which is strictly true only for the non-buoyant jet. This assumption will be valid for buoyant jets

if the mass per unit volume (or density) does not change appreciably from section to section in the jet (the Boussinesq approximation). This will be true except for sections close to the nozzle where there are large density differences. Using Equations 12, 13 and 14, the conservation of heat content becomes:

$$Q_o \Delta T_o = u_c \, \Delta T_c \int_A f_T^{\lambda^2+1} \, dA \tag{17}$$

Evaluating this for u_c and substituting it into Equation 15 gives:

$$S_V = \frac{\Delta T_o \int_A f_T^{\lambda^2} \, dA}{\Delta T_c \int_A f_T^{\lambda^2+1} \, dA} \tag{18}$$

By noting the definition of S_c, it can be seen that this equation relates S_V and S_c, by making use of a structural assumption about the jet. This had been proposed earlier in this discussion.

Substituting the distribution of temperature assumed in Equation 13 into Equation 18 yields

$$S_V = \frac{\int_A \left(\frac{\Delta T}{\Delta T_o}\right)^{\lambda^2} \, dA}{\int_A \left(\frac{\Delta T}{\Delta T_o}\right)^{\lambda^2+1} \, dA} \tag{19}$$

The advantage of this formulation for S_V is that it allows S_V to be evaluated by measuring only the temperature distribution, which is more easily and accurately measured than the velocity distribution.

This formulation also minimizes the error produced by the definition of the jet diameter. The jet diameter defines the limits of the numerical integration of measured temperature profiles in Equation 19 and small errors in the limits of integration will produce only small errors in S_V since the values of the temperature distribution at the edge of the jet are small.

By using these relationships for S_V and S_c, Equations 8 and 9 become:

$$S_V \text{ or } S_c = f(\frac{z}{d_o}, F, Re) \tag{20}$$

C. Results of Previous Investigations

All experimental studies of jet dilution have neglected Reynolds number effects and assumed fully developed turbulence in the jet. For the case of non-buoyant, turbulent axisymmetric jet, the volume dilution has been given by:

$$S_V = S_V^* \frac{z}{d_o} \tag{21}$$

where S_V^* = experimentally determined constant relating the rate of increase of S_V with respect to z/d_o

Values of S_V^* found by previous investigators are shown in Table 1. The value of S_V^* quoted by Daily and Harleman (9) for assumed Gaussian profiles is significantly less than that found for a constant value of the eddy viscosity. Since the velocities at the edge of the jet predicted by the Gaussian assumption were smaller than those actually found, the value of S_V^* for a constant eddy

Table 1

VALUES OF COEFFICIENT S_V^* FOUND

FOR NON-BUOYANT AXISYMMETRIC JETS

$$S_V = S_V^*\left(\frac{z}{d_o}\right)$$

Investigator	Reynolds #	$\frac{\rho_a}{\rho_o}$	Froude #	S_V^*	Comments
Abramovich (3)	Turbulent	1.00	∞	0.33	
Brooks (6)	Turbulent	1.00	∞	0.33	
Albertson et al	$\geq$1500	1.00	∞	0.32	air jets
Daily and Harleman (9)	70000	1.00	∞	0.42	based on Hinze constant eddy viscosity
Daily and Harleman (9)	70000	1.00	∞	0.28	Gaussian Assumption
Schlichting (21)	Laminar	1.00	∞	$\frac{32}{Re}$	

viscosity is a better estimation.

Also included in Table 1 is a boundary layer equation solution for the non-buoyant, laminar, axisymmetric jet, found by Schlichting (21). The expression for the volume flow rate is:

$$Q = 8\pi\nu z \tag{22}$$

Substituting this into Equation 10 yields

$$S_V = \frac{Q}{Q_o} = \frac{8\pi\nu z}{u_o \frac{\pi d_o^2}{4}} = \frac{32}{Re}\frac{z}{d_o} \tag{23}$$

Thus, for the laminar jet, this solution predicts $S_V^* = 32/Re$.

The centerline dilution for the non-buoyant, turbulent axisymmetric has been given by:

$$S_c = S_c^* \frac{z}{d_o} \tag{24}$$

where S_c^* = experimentally determined constant relating the rate of increase of S_c with respect to z/d_o

Values of S_c^* found by various investigators for the non-buoyant jet are given in Table 2.

For the buoyant, axisymmetric, turbulent jet, no previous studies have been found which calculate the volume dilution S_V. For the centerline dilution, previous investigators have used Equation 24 and evaluated S_c^*. Their results are shown in Table 3. The values of S_c^* given there are generally higher than those for

Table 2

VALUES OF COEFFICIENT S_c^* FOUND
FOR NON-BUOYANT AXISYMMETRIC JETS

$$S_c = S_c^* \left(\frac{z}{d_o}\right)$$

Investigator	Reynolds #	$\frac{\rho_a}{\rho_o}$	Froude #	S_c^*	Comments
Sunavala (22)	Turbulent	1.00	∞	0.220	Mixture of gases
Hinze, van der Hegge Zijnen(13)	Turbulent	1.01	∞	0.190	Mixture of gases
Forstall and Gaylord (11)	Turbulent	1.01	∞	0.192	Water jets salt solution
Ruden (20)	Turbulent	1.00	∞	0.170	Hot air jets
Becker, Hottel and Williams (5)	54,000	1.00	∞	0.185	Oil smoke in air jets
Corrsin and Uberoi (8)	11,400	~1.00	∞	0.185	Hot air jets
Keagy and Weller (16)	27,200	1.03	4300	0.170	Mixture of gases

Table 3

VALUES OF COEFFICIENT S_c^* FOUND

FOR BUOYANT AXISYMMETRIC JETS

$$S_c = S_c^* \frac{z}{d_o}$$

Investigator	Reynolds #	$\frac{\rho_a}{\rho_o}$	Froude #	S_c^*	Comments
Keagy and Weller (16)	5,020	0.65	1070	0.262	Mixture of gases
Keagy and Weller (16)	35,000	7.20	740	0.075	Mixture of gases
Sunavala, Hulse and Thring (23)	20,500	1.24	1470	0.238	Hot air jets
Sunavala, Hulse and Thring (23)	17,900	1.24	830	0.238	Hot air jets
Sunavala, Hulse and Thring	21,900	1.24	725	0.238	Hot air jets
Sunavala, Hulse and Thring (23)	24,600	1.24	620	0.238	Hot air jets
Corrsin and Uberoi (8)	39,400	~2.00	64	0.250	Hot air jets
Cleeves and Boelter	5,400	2.93	4	5.800	Hot air jets
Cleeves and Boelter (7)	1,805	2.24	10	2.600	Hot air jets
Cleeves and Boelter (7)	2,700	2.39	16	0.970	Hot air jets
Cleeves and Boelter (7)	4,770	2.35	28	0.600	Hot air jets
Cleeves and Boelter (7)	6,900	2.41	71	0.460	Hot air jets

the non-buoyant case in Table 2. The values of S_c^* calculated for the work of Cleeves and Boelter (7) are significantly higher than those of the other investigators. Their results may be affected by the fact that they used a length of pipe for the jet discharge rather than a nozzle, thus changing the initial velocity distribution from a uniform profile to a fully developed, turbulent profile. Also, their results may be affected by the use of very high nozzle temperatures (1200°F), which may have introduced Mach number effects, and by the presence of combustion at the nozzle caused by the method used to heat the air jets. Their work is presented to show the tendency for buoyancy to aid the rate of dilution increase.

D. Temperature as an Indicator of Dilution

Abraham (2) has shown theoretically, and supported experimentally, a general relationship between centerline dilution and distance from the nozzle as a function of densimetric Froude number, assuming a fully turbulent jet. His results are shown in Figure 3, where $F^{1/2}$ corresponds to the definition of Froude number used here, c_m/c_o corresponds to $1/S_c$ and x/d_o corresponds to z/d_o. This graph shows that buoyancy increases the centerline dilution for lower Froude numbers ($F < 15$-20). For higher Froude numbers, buoyancy is effective in increasing dilution only after a certain distance from the nozzle, below which the jet momentum is the primary mechanism causing turbulent diffusion and hence, dilution. This distance at which buoyancy becomes effective increases as the Froude number

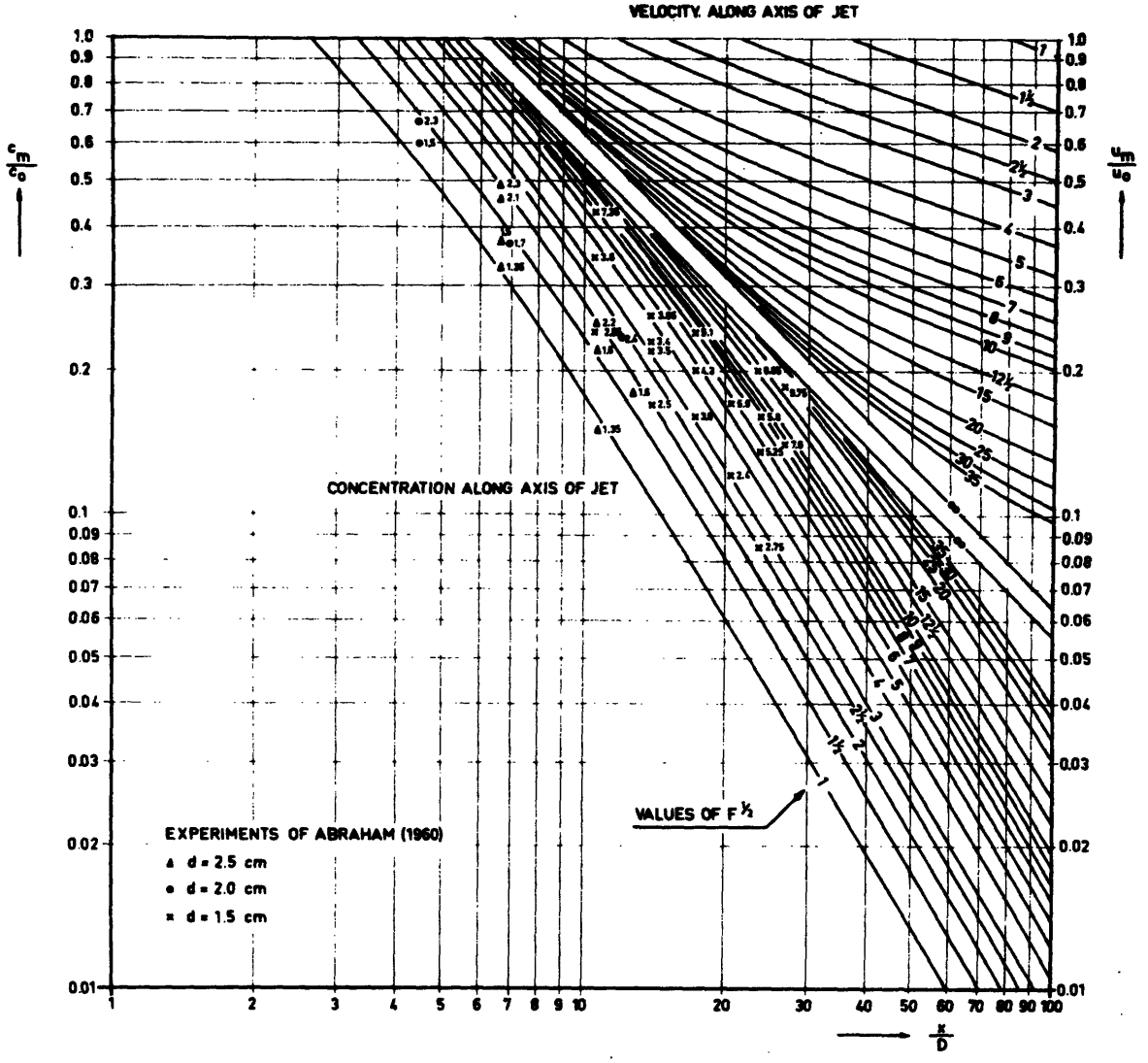

Figure 3. Concentration and velocity along axis of three dimensional jet (after Abraham(2))

increases.

Figure 3 forms the basis for using temperature as an indicator of jet dilution. Reynolds number effects on dilution for non-buoyant jets can be studied as long as all measurements are made below the distance after which buoyancy starts to aid dilution. Thus, experiments were chosen for densimetric Froude numbers of 10, 25, 50 and 100, each over a complete range of transition Reynolds numbers. Physical constraints limited testing to from 22 to 55 nozzle diameters above the jet. Figure 3 shows that Froude numbers of 50 and 100 are unaffected by buoyancy in this range. Thus, experiments for these Froude number values are the primary indicators of the effect of Reynolds number on dilution. Runs conducted at Froude numbers of 25 and 10 will be affected by buoyancy to an increasing extent. These results will be presented to document the effect of buoyancy in this range of transition Reynolds numbers.

V. Experimental Apparatus and Data Reduction

A. Apparatus

All experiments were conducted in the center section of a 3' deep 50' x 4.5' steel water tank. One side of the center section was constructed of glass so as to allow visual observation and photographs of experiments. The size of the tank was large enough to allow sufficient time to conduce experiments without stratification effects. A schematic of the experimental setup is shown in Figure 4.

All nozzles were mounted vertically on a copper tee in the central section of the tank. The copper tee allowed water to be supplied from opposite directions to offset any rotational or swirling effects in the jet. Nozzles of 1/8, 3/16, 1/4, 3/8, 1/2, and 3/4 inch diameter were constructed from copper reducer couplings to assure a fairly uniform velocity distribution at the nozzle exit. A picture of the nozzle apparatus is shown in Figure 5.

Hot water was supplied by a steam heat exchanger either through a constant heat tank or directly, if additional pressure was needed to maintain a sufficient flow rate. A by-pass line was installed to allow preliminary adjustment of temperature before water was issued into the tank. Flow was measured by means of individually calibrated Brooks low-flow rotameters with spherical floats. These flow meters, when individually calibrated, are accurate to $\pm$ 1% of full reading. Calibrations were performed using water with temperature typically encountered during experiments to minimize inaccuracies caused by temperature effects in the calibration.

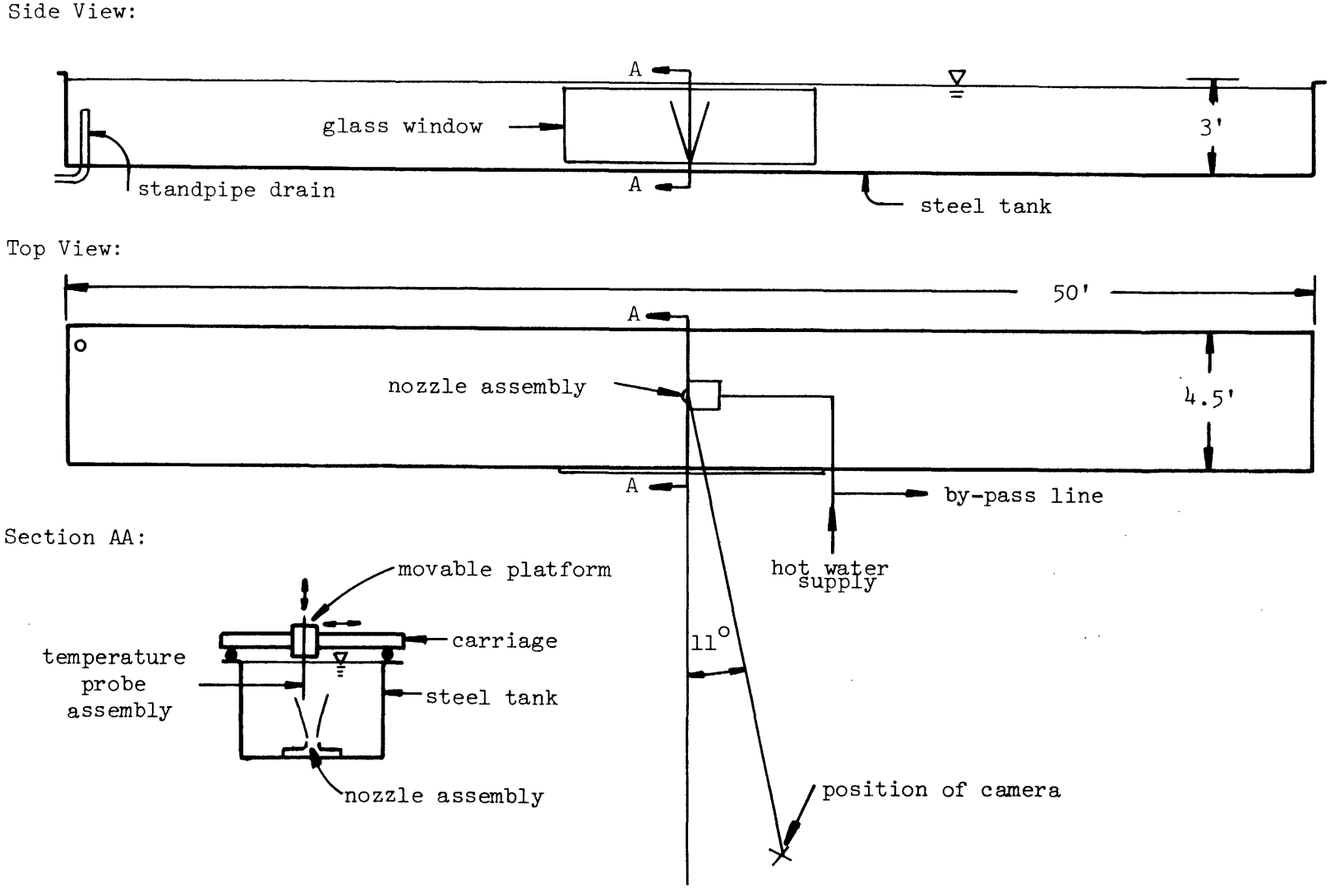

Figure 4. Schematic of Experimental Setup

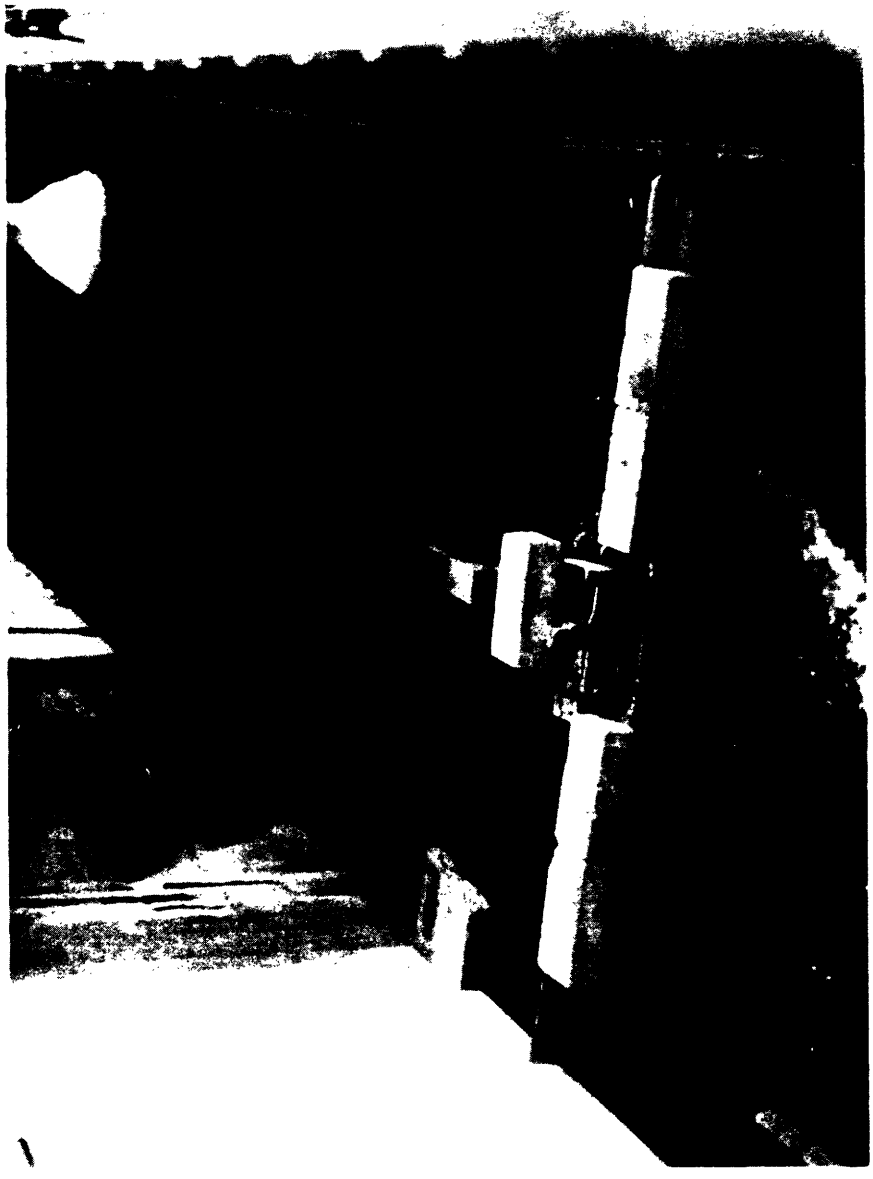

Figure 5. Nozzle Assembly

In addition, water passed through a cylinder of one cubic foot capacity before entering the tank, in order to reduce temperature oscillations and the presence of air bubbles in the hot water input, particularly when hot water was supplied directly from the steam heat exchanger. This cylinder reduced temperature oscillations to $\pm$ 0.8°F at the nozzle or about $\pm$ 4% of the temperature difference between the nozzle and the ambient fluid. The cylinder reduced the occasional presence of air bubbles to once every 5 or 10 minutes during these runs.

Temperature measurements were taken using a glass bead thermistor (Fenwal Electronics #GA51SM2) with a time constant of 0.07 seconds. The thermistor was calibrated in a constent temperature bath system to an accuracy of $\pm$ 0.02°F. The thermistor was mounted at the end of a vertically positioned length of 1/4" OD, thick walled copper tubing and encased in silicone construction sealant. The probe was mounted in a direction parallel to the tubing and located at a sufficient distance from the end of the tubing to allow the silicone sealant to be gently tapered to the outside diameter of the tubing. These precautions minimized the effect of the presence of the probe in the flow of the jet.

The probe and tubing were mounted in a Lory point gauge driven by a small D.C. motor. This motorized point gauge assembly was mounted on a rolling platform which traveled on a carriage supported by rails atop the tank walls. Both the platform and carriage were

driven by additional point gauge assemblies. The movement of all three gauges was converted to an electrical signal via a Bourne potentiometer.

The electrical signals from the temperature probe, an RMS meter and any one of the gauges were plotted by a Houston Instrument x-y-y' plotter. The RMS meter measured the fluctuations of the temperature signal and had a time constant of 2.0 seconds. The traversing speed of the gauges was adjusted to allow an accuracy of 1/16" on measurements of the RMS meter. This procedure assured virtually instantaneous temperature measurements.

Photographs of the experiments were made using a Topcon Super DM camera with a motorized drive and a 70-260mm Vivitar lens. Kodak black and white Tri-X film, ASA 400, was used with aperture f4 and shutter speed 1/60 second. The camera was located at a distance of 15 feet from the jet and at an angle of about 11° to the perpendicular from the tank wall, due to the presence of an obstacle along the perpendicular.

B. Experimental Procedure

Before experiments began, a computer program was developed which examined the sensitivity of the proposed range of densimetric Froude and Reynolds numbers to changes in the controlling parameters: nozzle diameter, flow rate, and the jet and ambient temperatures. On this basis an experimental program was outlined which would allow data to be collected with maximum ease and accuracy. Before any data was taken during an experiment, calculations of the Froude

and Reynolds numbers were made based on the actual reading to compare with desired values.

Temperature was initially adjusted, using the by-pass line, to a reading which would allow the desired jet temperature plus any flow rate dependent heat losses between the by-pass line and the nozzle. Final adjustments of flow rate and temperature were made based on the jet temperature measurement using the thermistor probe located at the nozzle exit. When the desired values of Froude and Reynolds number were reached, temperature profiles were made vertically along the jet axis and horizontally across the jet at distances of 7, 10, 15, 18, 22, 30 and 40 or 55 diameters from the nozzle. Several horizontal passes were made through the jet at each vertical level to insure the profiles close to or exactly on the jet axis was reached. Close watch was kept on the input temperature and flow rate to make sure that these values did not change significantly. After all measurements were made, warm dye (FD&C Blue #1, dissolved in water) was added to the jet and photographs were taken.

After each experiment, the water in the tank was either changed completely or the upper layers removed and additional water recirculated to remove all stratification effects. At least two hours was allowed between successive experiments to damp any velocity fluctuations in the tank.

C. Data Reduction

As stated previously, temperature measurements were recorded graphically in the form of a vertical axial profile and several horizontal profiles at various vertical distances from the nozzle. From the horizontal profiles, the plot which showed the highest peak temperature was chosen as the plot closest to the jet axis at that distance. Figure 6a shows a typical series of horizontal profiles and the plot chosen for use. Comparison of the peak temperatures on each of these plots with the corresponding point on the axial profile showed that the axial plot was never completely on the jet centerline. Thus, the horizontal profiles were used to provide all the data on each experiment.

After the appropriate profiles were selected, a line was drawn through each profile, from which data points were taken either by hand or by an x-y digitizer for eventual use by computer. Figure 6c shows four typical profiles in the range of Froude numbers encountered in experiments, indicating the degree of temperature fluctuation in the profiles, the method of determining the line from which data points were taken for the temperature profile, and the method of determining the jet diameter for a profile. Placement of the line giving the profile data points was accomplished by noting the average value of the temperature at a particular point and by studying the profile, particularly those at lower Froude numbers, for intermittency or points of low temperature

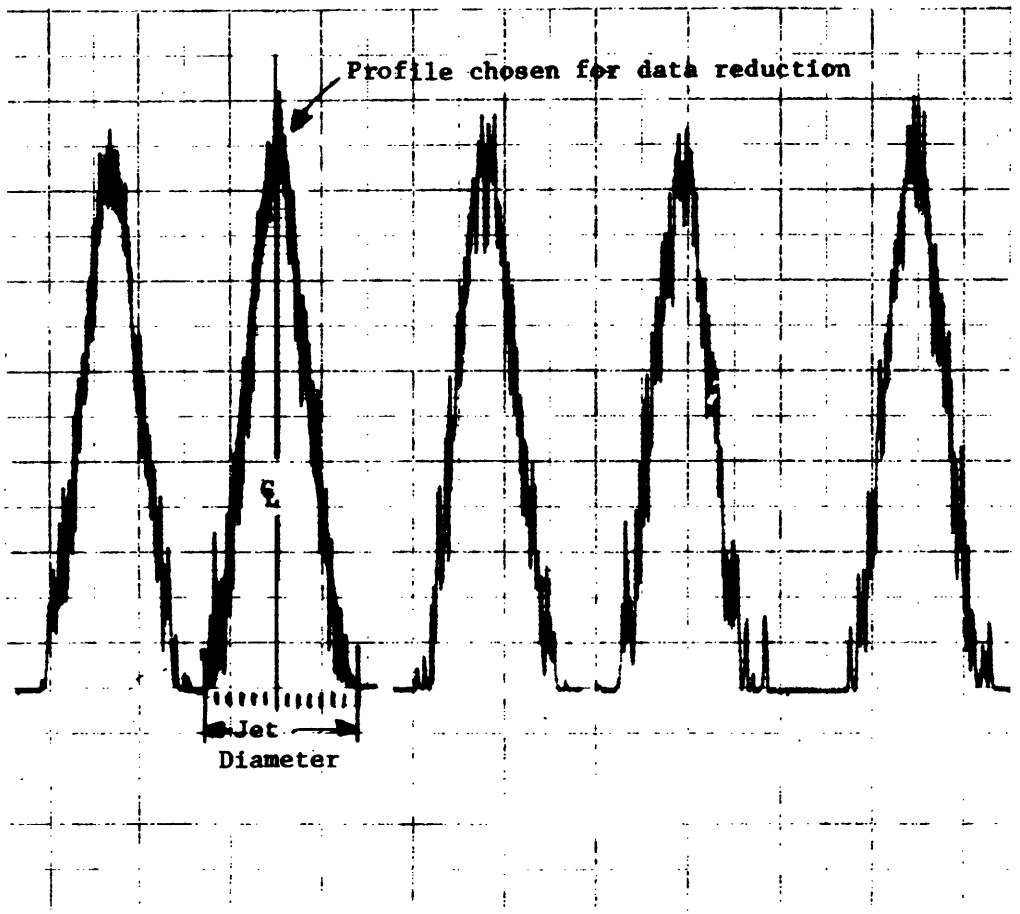

Figure 6a.
Selection of Best Profile from a Number of Traverses
at $z/d_o = 10$

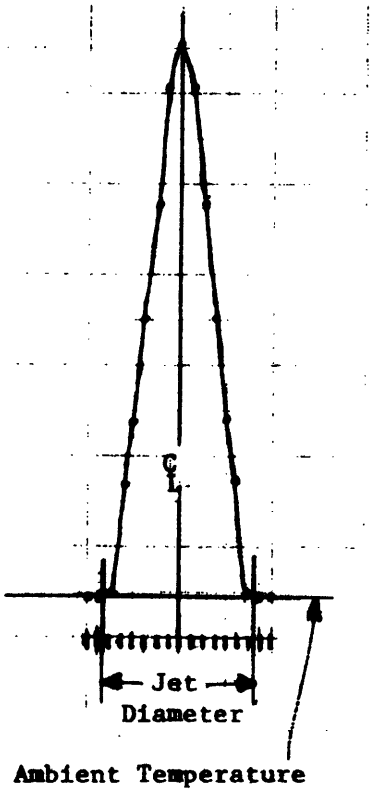

Figure 6b.
Radial Profile
obtained from Figure 6a.

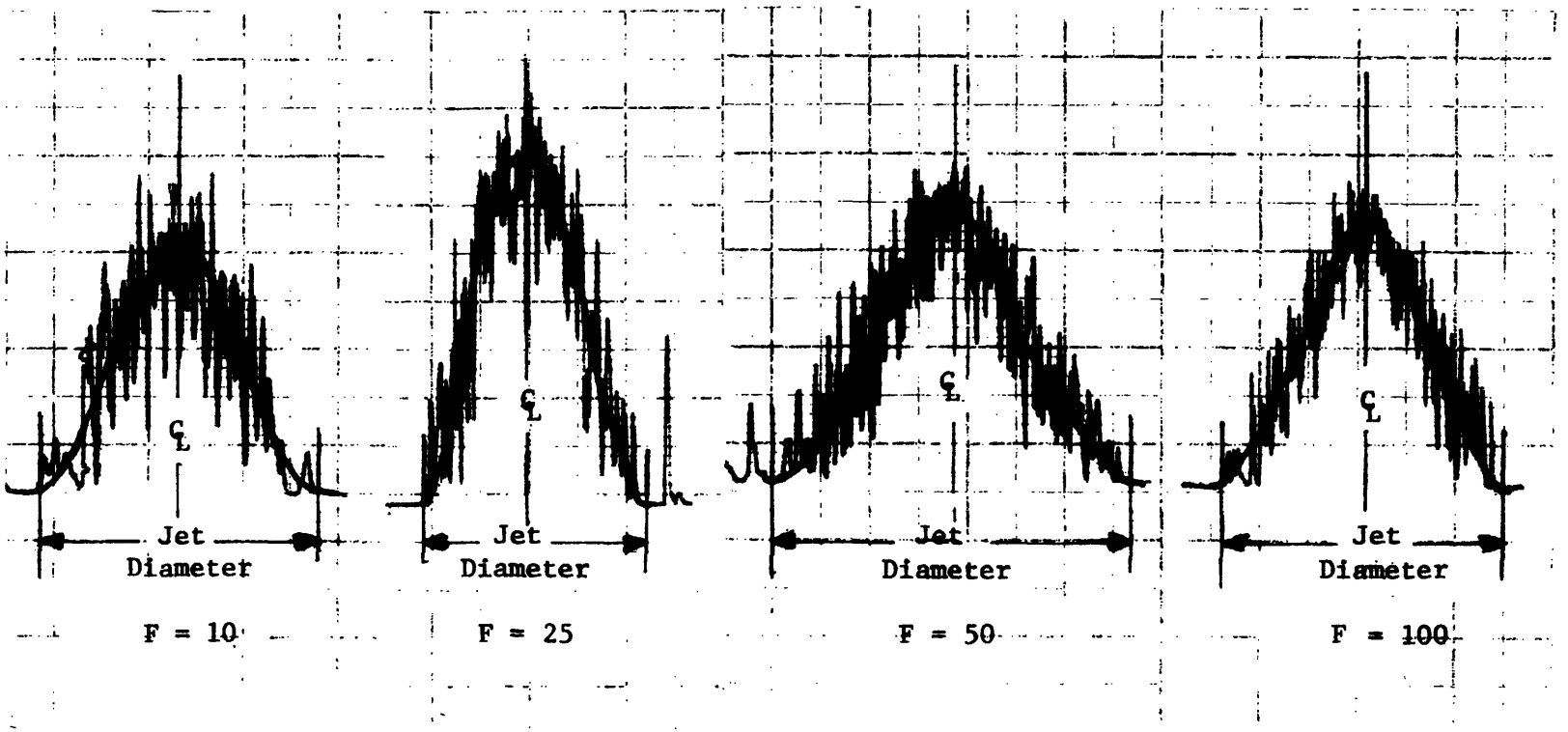

Figure 6c.
Examples of Temperature Fluctuation, Jet Diameter Definition and Mean Profiles
for various Froude Numbers

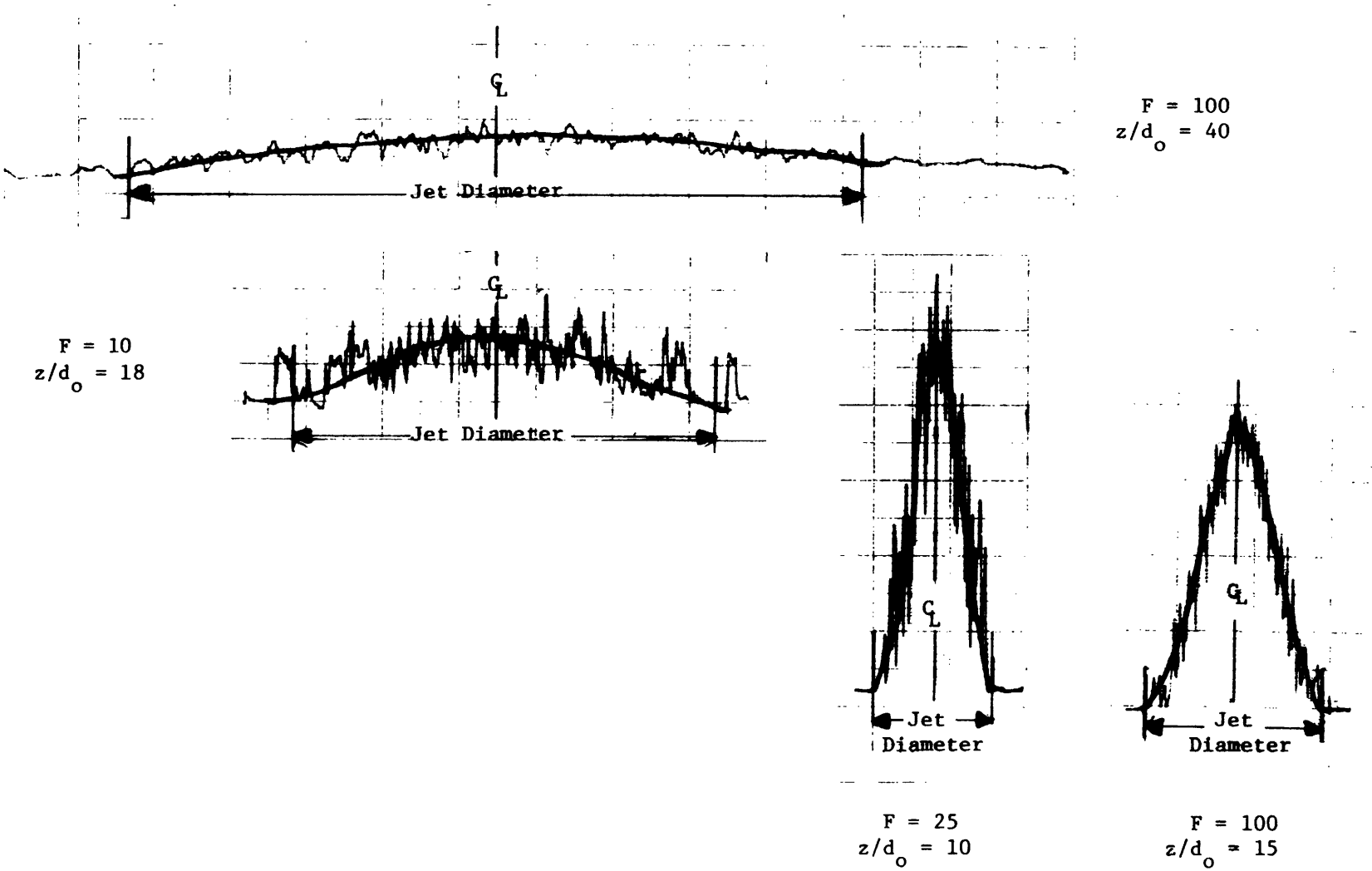

Figure 6d. Examples of Definition of Diameter

fluctuation which indicated the passage of an eddy by the thermistor probe. Definition of the edge of the jet was given by the intersection of the temperature profile with the local ambient temperature. After a profile was digitized, the temperature was averaged about the point of peak temperature to produce a plot of temperature versus radial distance, from which all parameters were calculated. Figure 6b shows the result of this process for the profile chosen in Figure 6a.

A computer program was developed to compute all parameters. Calibration plots and density and viscosity curves were internally stored in order to calculate Froude and Reynolds numbers and all dilution parameters directly. The limits of integration of the temperature profiles were based on the jet radius defined above. Particular profiles which were influenced by stratification in the tank were eliminated when calculating characteristic parameters. A profile was considered to be influenced by stratification whenever the local ambient temperature of the profile rose significantly above the constant ambient temperature in the lower layer of the tank. Thus, profiles were eliminated when:

$$\frac{T_{al} - T_a}{T_c - T_a} \geq 0.1 \qquad (25)$$

where T_{al} = local ambient temperature

Photographs were analyzed to obtain the laminar length and cone angle for each experiment. The laminar length, z_1/d_o, was

measured using a linear scale, which was drawn on the glass window of the tank and which appeared in each picture. The cone angle, $2\alpha_t^o$, was measured using Pearce's method of drawing a straight line as a mean through the irregular vortex boundary of the turbulent section of each jet. Pearce noted that this line could instead by drawn through the very outer edge of the vortices and then obtain a larger value of the cone angle. Since he was not concerned with the absolute magnitude of $2\alpha_t^o$, but rather with its relative variation with Reynolds number, he chose to use the mean line through the boundary.

D. Sources of Error

1. Sources of error in flow measurement

Previous mention was made of efforts to minimize errors caused by swirling effects in the jet, by the shape of the nozzle, by flow rate fluctuations, by temperature effects in flow calibrations and by the presence of air bubbles. Additional errors might have been caused by the presence of walls 27" on either side of the nozzle, but this seems doubtful after close observations of dye patterns during experiments. An additional source might be the fact that all nozzles projected from the bottom of the tank rather than issuing from a point flush with the tank bottom, thus possibly providing increased access of the jet to ambient water for entrainment. Pearce's study of the difference between flush and projecting nozzles was inconclusive; therefore, this effect does not seem to be important.

2. Sources of error in temperature regulation and measurement

The description of experimental equipment outlines efforts to minimize the effect of the temperature probe in the jet, the effect of stratification in the tank, and the effect of oscillating temperatures from the steam heat exchanger. The asymmetry in some of the profiles taken can be explained by several factors: the stochastic nature of turbulence in the jets; the effect of the probe time constant, although this was appreciably minimized by the low traversal speed used; and by probe interference, particularly at low Reynolds numbers.

The accuracy of the profiles could also be affected by the method for determining the average profile from the graphic output. In addition, the profiles might have been affected by the relative temperature measurement error for low temperature differences. Given the absolute accuracy of the probe is $\pm$ 0.02°F, temperature differences less than 0.5°F will decrease accuracy to greater than 4%. This may be particularly important at the edges of the jet and at distanced far from the jet. However, the diameter of the jet taken from the profiles was never used directly in the data reduction except for defining the limits of integration of the profiles, as discussed earlier. Also, physical constraints eliminated the possibility of using temperature measurements far from the jet.

3. Sources of error in photographs

All photographs recorded an image that was about 10% smaller

than the actual jet because of refraction effects due to the camera angle. Absolute distance measurements were made by means of a linear scale placed on the glass window of the tank and also recorded in the pictures. Measurements from this scale were about 2% larger than the image recorded by the camera, again due to the camera angle. This error slightly offset refraction effect errors.

These errors particularly affected the measurement of the laminar length from photographs, but did not have significant effect on the cone angle measurements, since they are not dependent on scale. While the errors in experimental photographs are larger than those for other parts of the experimental setup, they will not be particularly significant because the pictures are not used to show agreement in an absolute sense with other investigators. This argument is the same used by Pearce in his discussion of the accuracy of photographs, mentioned earlier.

4. General discussion of errors

It must be noted that all of the effects mentioned above varied in importance depending on the particular parameters of each experiment. Flow rate fluctuations and the presence of air bubbles were more important when the steam heat exchanger was connected directly to the nozzle rather than through the constant head tank, for runs where a high flow rate through a small nozzle was required. The interference of the temperature probe was relatively more important during runs of low Reynolds number when the jet included

a laminar length. This probably caused some asymmetry in the profiles. Determining the average profile was more difficult for low Froude number runs because of an increased level of temperature fluctuation, as shown in Figure 6c. Definition of the jet radius as the intersection of the profile with the local ambient temperature was more difficult for profiles at large distances from the nozzle than for those closer to the nozzle, as shown in Figure 6d. The former, however, were usually eliminated due to stratification effects.

VI. Results and Discussion

A. General Presentation of Results

The general results of all runs are given in Tables 4-7. Each table is a grouping of approximately equal Froude number experiments listed in order of increasing Reynolds number. For each experiment, a regression analysis was performed by computer to calculate the equation which best fit the data for Equations 21 and 24. In addition, regression analysis was performed on Abraham's (2) equation relating centerline dilution and distance for non-buoyant jets, adapted as follows:

$$\frac{1}{S_c} = C_1 \left(\frac{d_o}{z}\right)^n \tag{26}$$

Correlation coefficients indicating goodness of fit are also listed. The correlation coefficients are defined as:

$$cc = \left(\frac{SSR}{SST}\right)^{1/2} \tag{27}$$

where SSR = sum of the squares due to the regression

SST = total sum of the squares due to raw data

Figure 7 compares the results of this study for the fully turbulent runs of Re = 4000 with Abraham's results of Figure 3 for the various densimetric Froude numbers. An increase in dilution for increasing Froude numbers is shown. This variation of dilution with Froude number is similar to that predicted by

Table 4

EXPERIMENTAL RESULTS FOR FROUDE NUMBER = 100

cc = correlation coefficient			$\frac{1}{S_c} = C_1 (\frac{d_o}{z})^n$			$S_c = S^*_c \frac{z}{d_o}$		$S_V = S^*_V \frac{z}{d_o}$					
								$\lambda^2 = 1$			$\lambda^2 = 2$		
Run #	Froude #	Reynolds #	C_1	n	cc	S^*_c	cc	S^*_V	cc	$\frac{S^*_V}{S^*_c}$	S^*_V	cc	$\frac{S^*_V}{S^*_c}$
23	122.8	1223	13.30	1.28	0.994	0.183	0.995	0.299	0.965	1.63	0.239	0.974	1.31
21	131.6	1528	9.74	1.26	0.996	0.308	0.997	0.571	0.997	1.85	0.697	0.952	2.26
22	113.7	2259	4.40	0.95	0.990	0.208	0.988	0.352	0.998	1.69	0.304	0.995	1.46
32	101.2	4043	5.21	1.01	0.998	0.204	0.997	0.317	0.999	1.55	0.279	0.999	1.37
30	86.6	4538	3.26	0.86	0.994	0.192	0.993	0.311	0.996	1.62	0.269	0.996	1.40
13	96.0	5263	2.21	0.77	0.998	0.204	0.986	0.428	0.994	2.10	0.345	0.995	1.69
3	91.5	10496	4.44	0.94	0.998	0.185	0.999	0.309	0.996	1.67	0.253	0.999	1.37
35	94.1	18287	5.08	1.03	0.998	0.206	0.997	0.358	0.998	1.74	0.312	0.994	1.51
4	99.4	18934	4.07	0.89	0.993	0.153	0.998	0.270	0.992	1.76	0.217	0.996	1.42

Table 5

EXPERIMENTAL RESULTS FOR FROUDE NUMBER = 50

cc = correlation coefficient			$\frac{1}{S_c} = C_1(\frac{d_o}{z})^n$			$S_c = S_c^* \frac{z}{d_o}$		$S_V = S_V^* \frac{z}{d_o}$					
								$\lambda^2 = 1$			$\lambda^2 = 2$		
Run #	Froude #	Reynolds #	C_1	n	cc	S_c^*	cc	S_V^*	cc	$\frac{S_V^*}{S_c^*}$	S_V^*	cc	$\frac{S_V^*}{S_c^*}$
24	56.8	479	1.82	0.34	0.982	0.035	0.967	0.127	0.969	3.64	0.089	0.967	2.54
18	57.3	794	11.00	1.26	0.976	0.240	0.981	0.391	0.986	1.63	0.348	0.977	1.45
19	52.0	1007	8.94	1.25	0.990	0.259	0.993	0.447	0.999	1.73	0.413	0.997	1.60
20	47.7	1604	4.38	0.98	0.998	0.206	0.999	0.364	0.996	1.76	0.305	0.997	1.48
16	49.2	2567	3.93	0.92	0.998	0.188	0.996	0.336	0.987	1.79	0.277	0.997	1.47
2	49.6	3608	3.84	0.89	0.997	0.156	0.991	0.299	0.997	1.92	0.240	0.998	1.54
7	49.3	9857	2.61	0.80	0.993	0.183	0.996	0.315	0.991	1.72	0.258	0.994	1.41
8	48.7	11447	3.06	0.87	0.997	0.188	0.997	0.357	0.999	1.90	0.290	0.998	1.54

Table 6

EXPERIMENTAL RESULTS FOR FROUDE NUMBER = 25

cc = correlation coefficient			$\frac{1}{S_c} = C_1(\frac{d_o}{z})^n$			$S_c = S_c^* \frac{z}{d_o}$		$S_V = S_V^* \frac{z}{d_o}$					
								$\lambda^2 = 1$			$\lambda^2 = 2$		
Run #	Froude #	Reynolds #	C_1	n	cc	S_c^*	cc	S_V^*	cc	$\frac{S_V^*}{S_c^*}$	S_V^*	cc	$\frac{S_V^*}{S_c^*}$
27	32.9	109	6.18	0.79	0.846	0.105	0.872	0.143	0.945	1.36	0.102	0.931	0.97
25	28.8	342	9.83	0.99	0.836	0.164	0.903	0.216	0.917	1.32	0.195	0.914	1.19
26	20.9	519	8.24	0.99	0.882	0.169	0.920	0.242	0.982	1.43	0.223	0.974	1.32
17	24.1	662	0.15	1.45	0.961	0.422	0.985	0.701	0.985	1.66	0.585	0.986	1.39
29	26.1	1079	6.89	1.15	0.997	0.236	0.999	0.327	0.984	1.38	0.292	0.987	1.24
15	24.2	1304	8.09	1.14	0.995	0.227	0.991	0.301	0.943	1.32	0.273	0.983	1.20
1	27.2	2124	4.40	0.94	0.998	0.173	0.998	0.294	0.977	1.70	0.249	0.992	1.44
6	24.3	3967	2.71	0.83	0.988	0.205	0.993	0.337	0.999	1.64	0.294	0.996	1.47
10	23.9	8228	2.45	0.78	0.998	0.181	0.996	0.375	0.997	2.07	0.299	0.999	1.65

Table 7

EXPERIMENTAL RESULTS FOR FROUDE NUMBER = 10

cc = correlation coefficient			$\frac{1}{S_c} = C_1(\frac{d_o}{z})^n$			$S_c = S_c^* \frac{z}{d_o}$		$S_V = S_V^* \frac{z}{d_o}$					
								$\lambda^2 = 1$			$\lambda^2 = 2$		
Run #	Froude #	Reynolds #	C_1	n	cc	S_c^*	cc	S_V^*	cc	$\frac{S_V^*}{S_c^*}$	S_V^*	cc	$\frac{S_V^*}{S_c^*}$
14	8.1	338	17.90	1.26	0.892	0.245	0.941	0.345	0.976	1.41	0.310	0.965	1.26
28	10.5	475	2.87	0.49	0.807	0.056	0.875	0.159	0.924	1.56	0.100	0.885	1.78
33	10.4	712	28.00	1.60	0.985	0.415	0.978	0.688	0.980	1.66	0.637	0.966	1.53
34	10.0	1080	13.60	1.38	0.980	0.330	0.977	0.451	0.969	1.37	0.419	0.973	1.27
5	8.8	1447	4.41	0.94	0.997	0.188	0.997	0.256	0.962	1.36	0.249	0.993	1.32
9	9.9	1934	2.77	0.86	0.989	0.220	0.994	0.310	0.966	1.41	0.290	0.984	1.32
31	10.1	3150	3.19	0.94	0.991	0.265	0.996	0.411	0.995	1.55	0.359	0.997	1.36
11	10.0	4013	2.20	0.87	0.996	0.273	0.995	0.476	0.970	1.75	0.379	0.984	1.39
12	8.9	5151	2.04	0.83	0.998	0.268	0.997	0.386	0.993	1.44	0.349	0.992	1.30

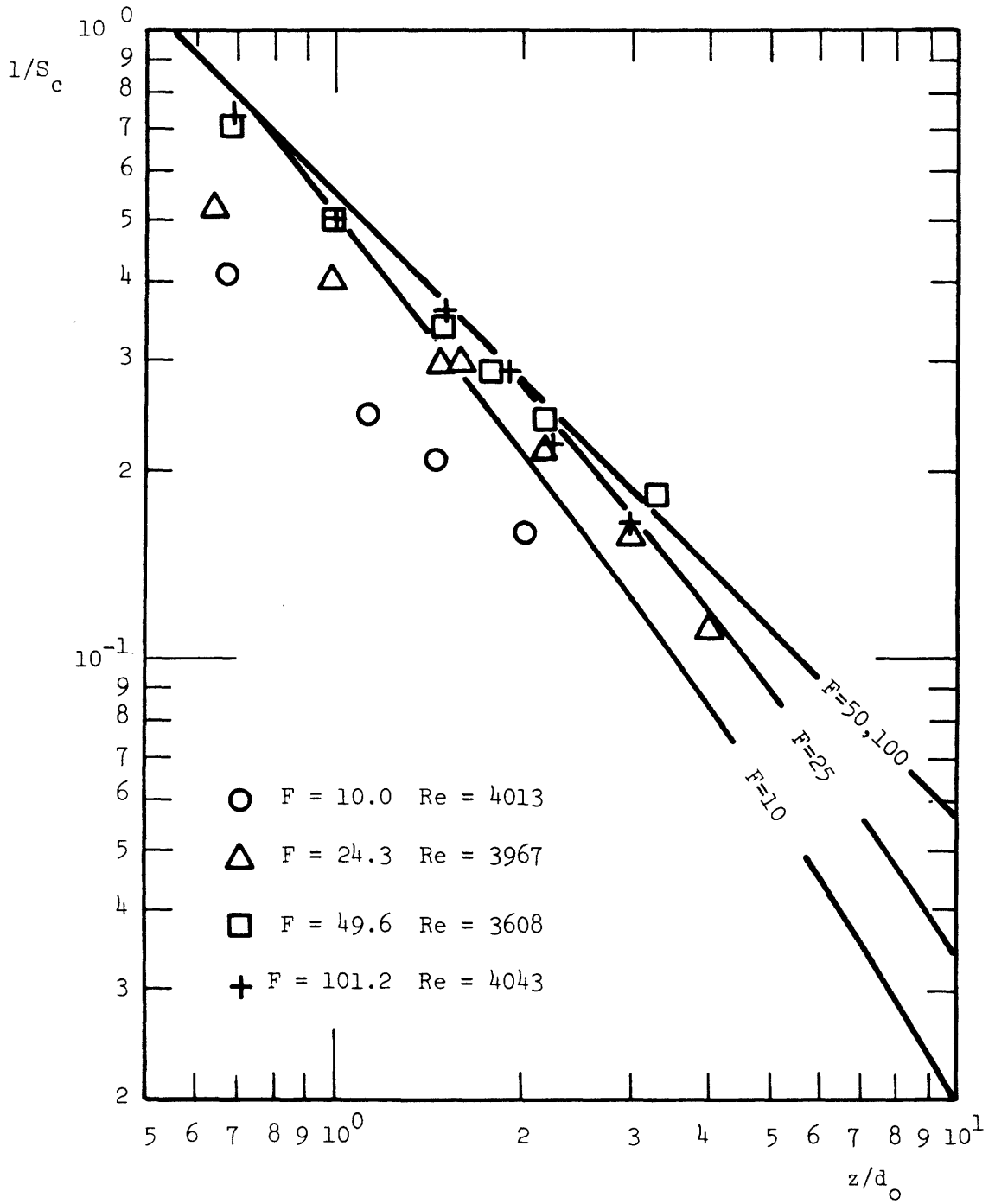

Figure 7. Inverse Centerline Dilution versus z/d_o for Non-buoyant and Buoyant Turbulent Jets

Abraham, although all Froude numbers show a higher dilution than those given by Figure 3.

B. Non-buoyant Jets

Inspection of both Tables 4 and 5 will show two generally different types of behavior for non-buoyant jets. Runs of Reynolds number below 1500 have a larger exponent for Equation 26 than those above Re = 1500, which conform closer to Abraham's results: $4.0 < C_1 < 6.0$ and $n = 1.0$. This change in behavior can again be seen by examining Figure 8, which shows S_c versus Re for $z/d_o = 15$ and F = 50 and 100. Dilution conforms fairly well to a value postulated by Abraham until a Reynolds number of about 1000-1500, below which dilution decreases.

Figure 9 shows the coefficient S_c^* plotted versus Reynolds number for Froude numbers of 50 and 100. These results show fairly good agreement with values found by investigators listed in Table 2 for Reynolds numbers above 1500.

Tables 4 and 5 also give S_V^* for F = 50 and 100 and two different assumptions with respect to λ. These results show fairly good agreement with the values given in Table 1 for the similarity assumption of $\lambda^2 = 1$ for Reynolds numbers above 1500. Although the values of S_V^* are lower for $\lambda^2 = 2$, the difference is not significant. For round turbulent jets, and utilizing Gaussian profiles, Equation 18 gives:

$$\frac{S_V}{S_c} = \left(\frac{1 + \lambda^2}{\lambda^2}\right) \tag{28}$$

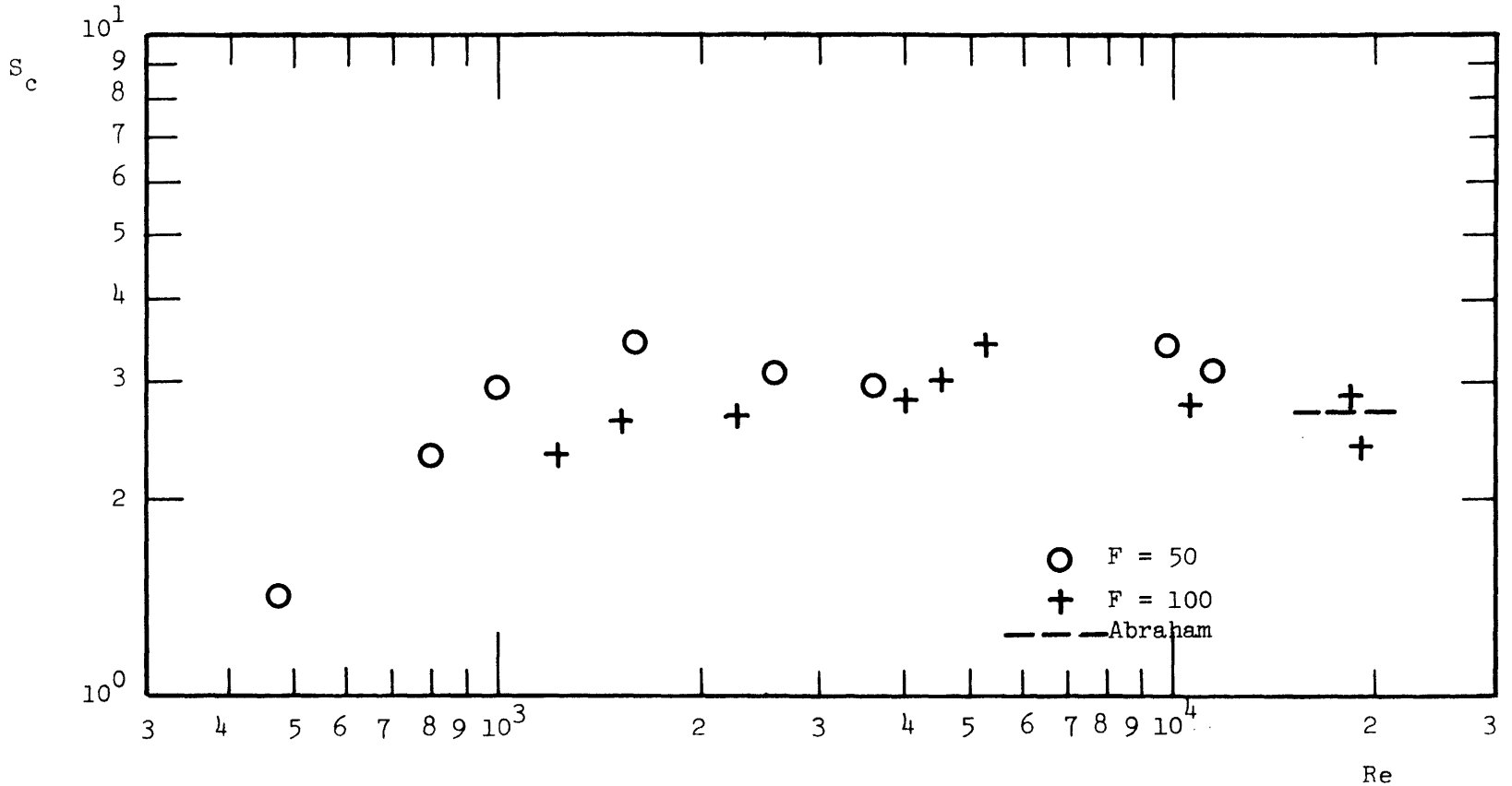

Figure 8. S_c versus Reynolds Number for Non-buoyant Jets at $z/d_o = 15$

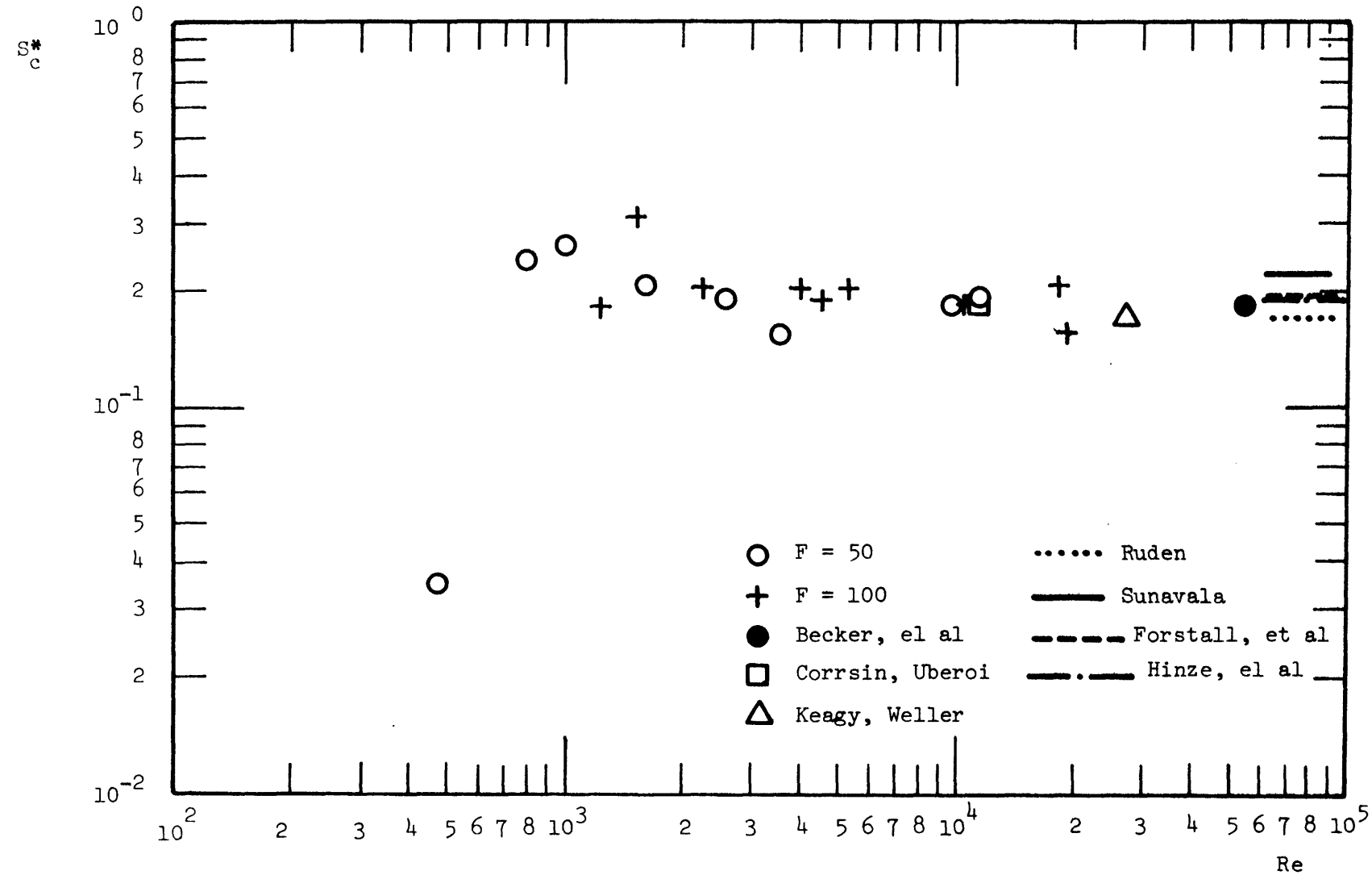

Figure 9. S_c^* versus Reynolds Number for Non-buoyant Jets

For $\lambda^2 = 1$ and $\lambda^2 = 2$, S_V/S_c should equal 2.0 and 1.5, respectively. Using Equations 21 and 24, this can be expressed as:

$$\frac{S_V}{S_c} = \frac{S_V^*}{S_c^*} \tag{29}$$

Computation of this ratio, also shown in Tables 4 and 5, reveals experimental values that are roughly 20% higher for $\lambda^2 = 1$, but which agree favorably for $\lambda^2 = 2$, especially for Reynolds numbers above 1500. Thus it seems that Taylor's assumption that $\lambda^2 = 2$ for turbulent jets is supported by these results for non-buoyant jets. Figure 10 shows S_V^* plotted versus Reynolds number.

Table 8 gives the results of the analysis of the photographs for these runs. Figures 11 and 12 plot laminar length and cone angle, respectively, versus Reynolds number. Pearce's results for convergent nozzles are also plotted on each graph, as well as the envelope for results using parallel sided nozzles.

The data of this study shows general agreement with that of Pearce's convergent nozzles. Pearce pointed to the difference in initial velocity profiles for convergent and parallel sided nozzles to explain the increased scatter of Figures 11 and 12. In a convergent nozzle, the velocity profile at the entrance is uniform, while in a parallel sided nozzle, the velocity profile is fully developed. In the process of establishing similarity profiles in the jet flow, a uniform profile would tend to generate greater shear

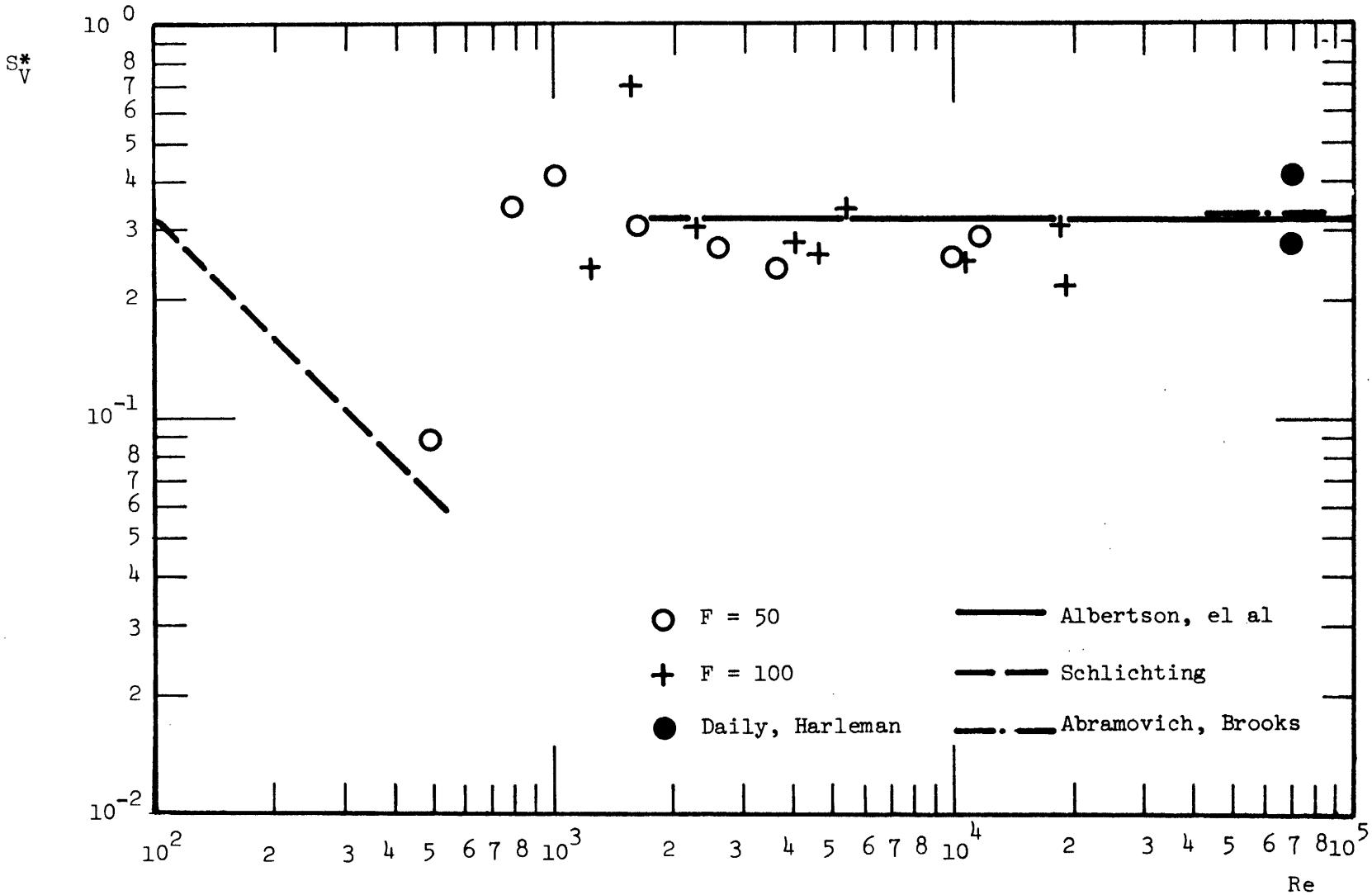

Figure 10. S_V^* versus Reynolds Number for Non-buoyant Jets ($\lambda^2 = 2$)

Table 8

LAMINAR LENGTH AND CONE ANGLE FOR NON-BUOYANT JETS

Froude Number = 50						Froude Number = 100					
Run #	Froude #	Reynolds #	Diameter (inches)	Laminar Length z_1/d_o	Cone Angle $2\alpha_t^o$	Run #	Froude #	Reynolds #	Diameter (inches)	Laminar Length z_1/d_o	Cone Angle $2\alpha_t^o$
24	56.8	479	0.125	13.0	21°	23	122.8	1223	0.125	4.0	21°
18	57.5	794	0.125	9.0	25°	21	131.6	1528	0.125	3.0	23°
19	52.0	1007	0.125	8.0	23°	22	113.7	2259	0.125	0	20°
20	47.7	1604	0.125	3	21°	32	101.2	4043	0.125	0	20°
16	49.2	2567	0.1875	2	20°	30	86.6	4538	0.1875	0	20°
2	49.6	3608	0.25	0	21°	13	96.0	5263	0.1875	0	19°
7	49.3	9857	0.375	0	21°	3	91.5	10496	0.25	0	17°
8	48.7	11447	0.375	0	20°	35	94.1	18287	0.25	0	20°
						4	99.4	18934	0.25	0	21°

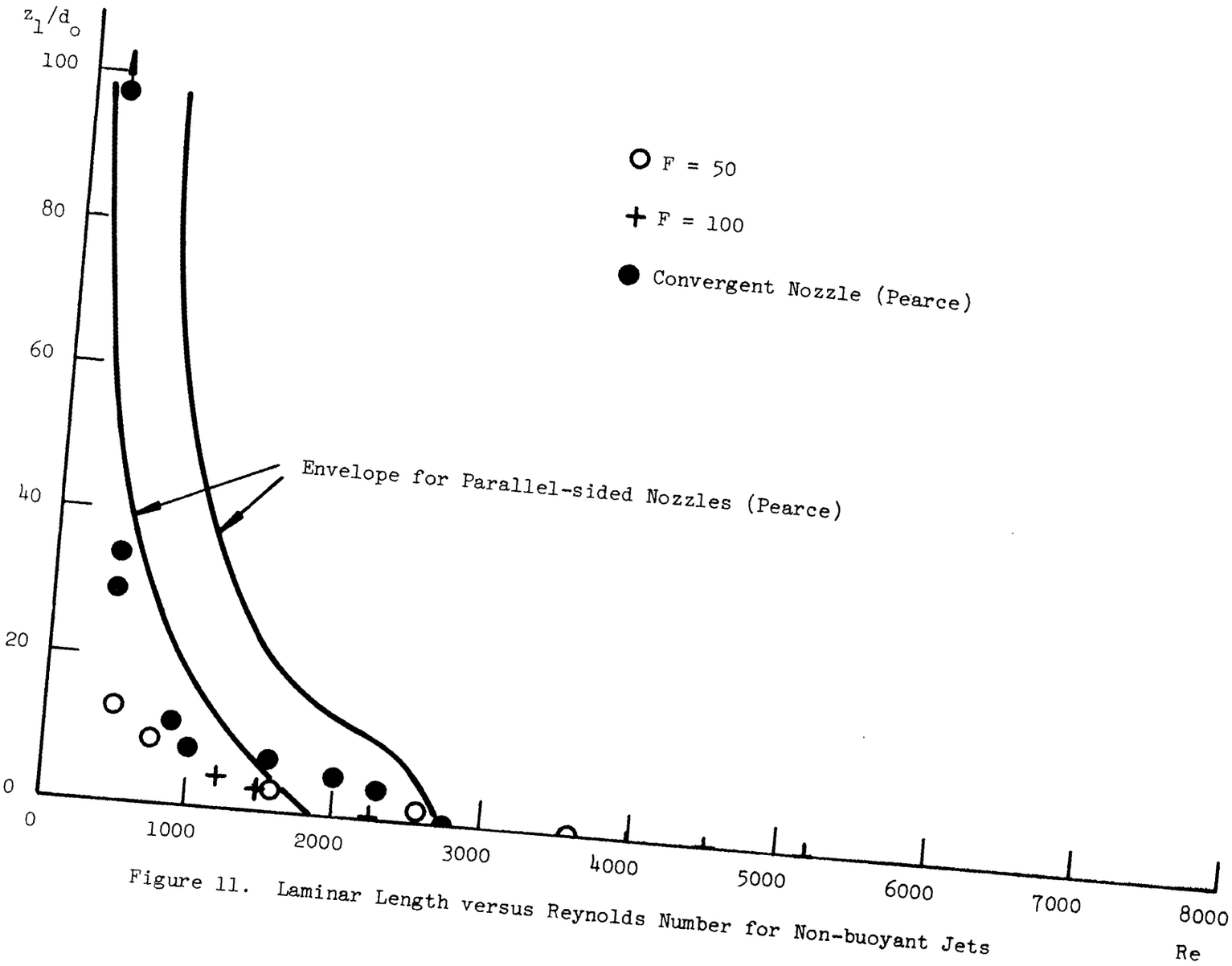

Figure 11. Laminar Length versus Reynolds Number for Non-buoyant Jets

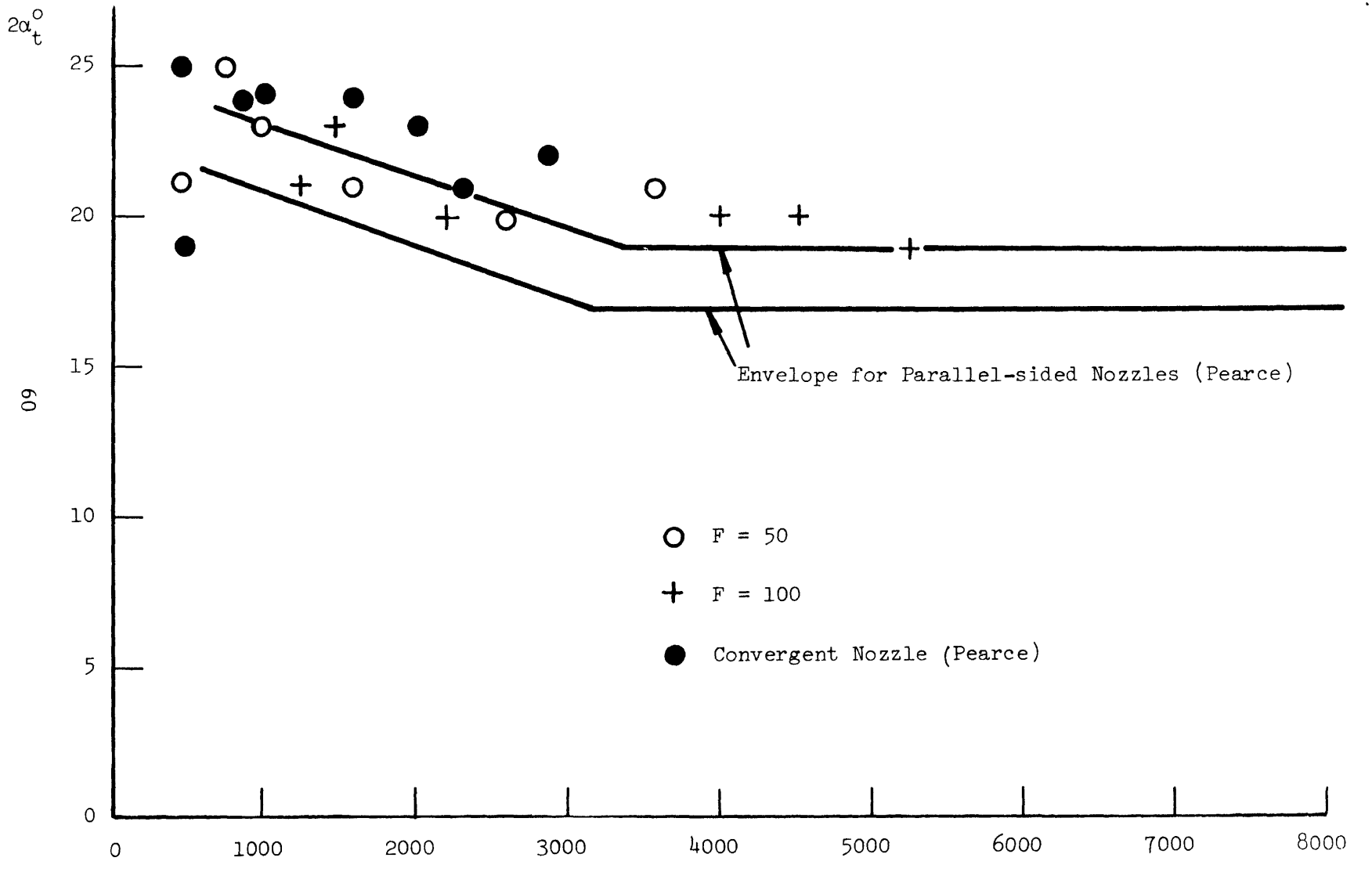

Figure 12. Cone Angle versus Reynolds Number for Non-buoyant Jets

and thus entrain more ambient fluid than a fully developed profile. Lateral spread of velocity and temperature distributions would be more rapid. This is confirmed by the larger cone angles for the convergent nozzles compared to the parallel sided nozzles.

Because of the increased scatter of the cone angle data, Pearce relied mainly on the laminar length to make his conclusion that a jet is fully turbulent for Re > 3000. The data of this study for the laminar length support a slightly lower Reynolds number above which a jet is fully turbulent. The values of the laminar length found in the experiments are generally lower than those of Pearce but the laminar length is always of the order of the length of the turbulent potential core for Re > 1500. The slight difference is probably due to the photographic distortion discussed earlier, but since relative changes in laminar length versus Reynolds number are mainly of interest, the conclusion supporting a lower critical Reynolds number is still valid.

Figure 13 shows photographs of non-buoyants for a range of Reynolds numbers. They compare favorably to the pattern of transition noted by Pearce, and described in Chapter III. The jets had a laminar length until about 2000 < Re < 2500. The resistance to instability was noted by Pearce for Re < 500. The experimental data in that range does not support his statement, but the general lack of runs in that range cannot support a different conclusion.

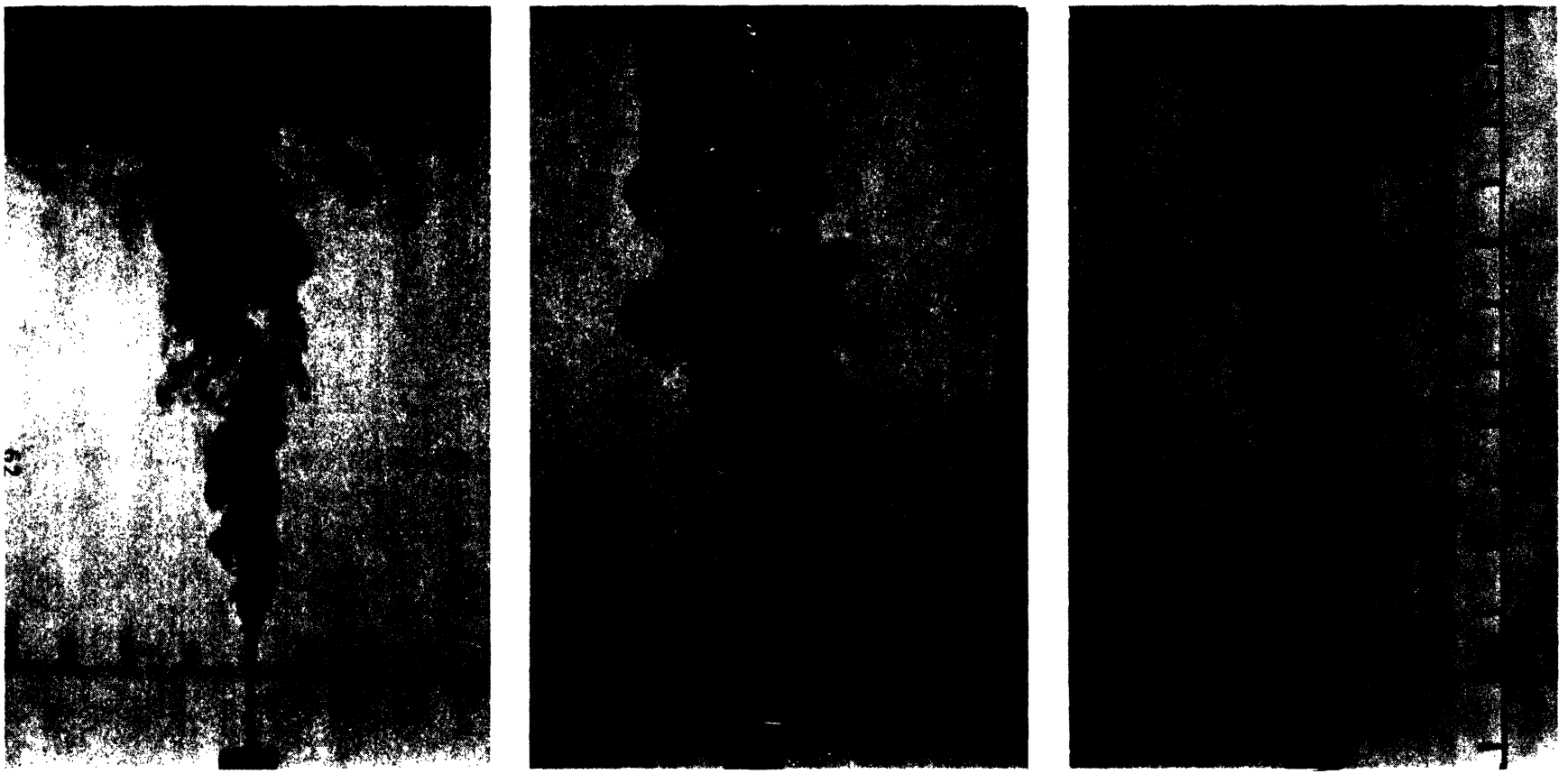

Re = 479
Run #24

Re = 794
Run #18

Re = 1007
Run #19

Figure 13. Examples of Non-buoyant Jets

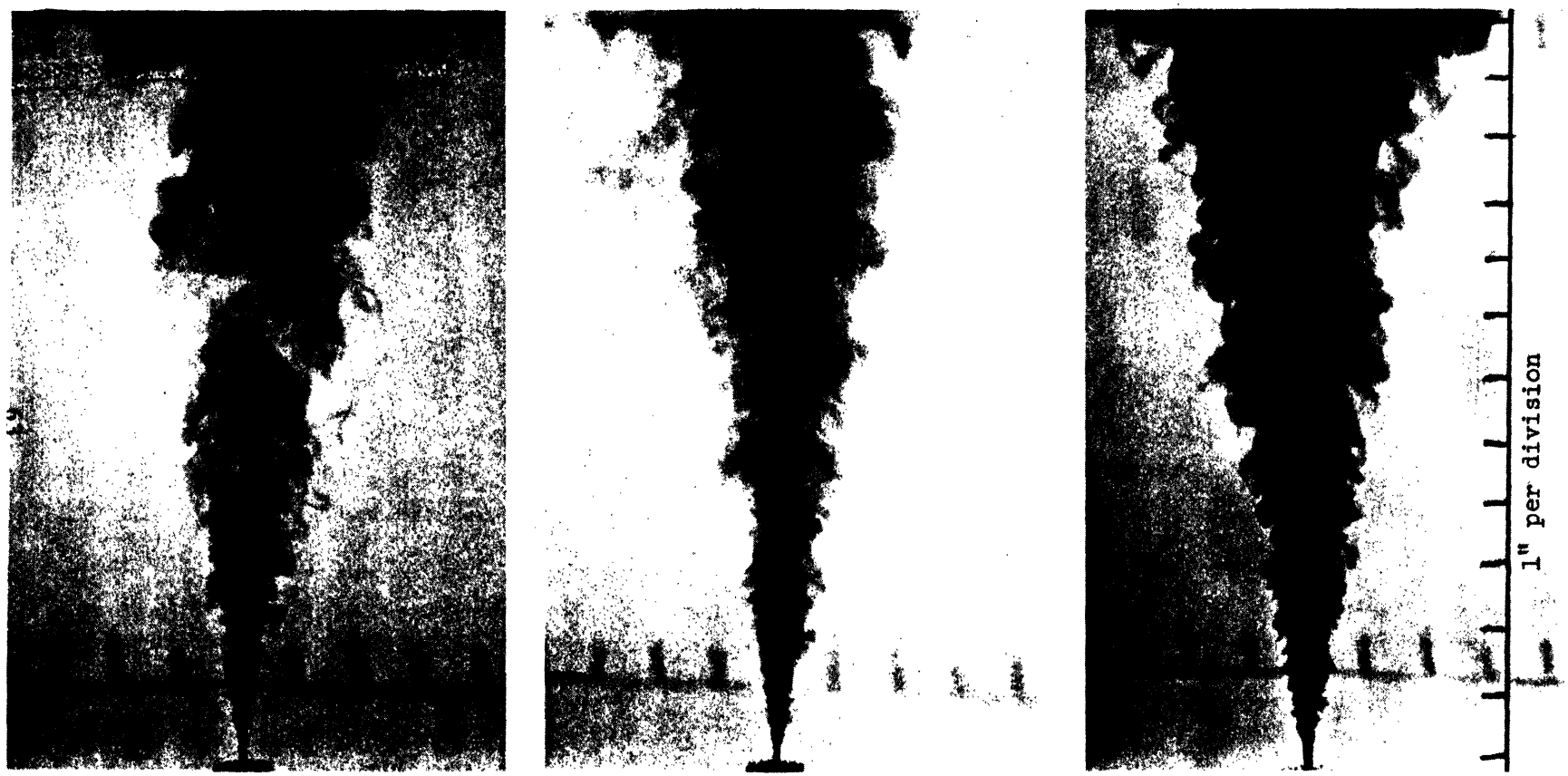

Re = 1604
Run #20

Re = 2259
Run #22

Re = 2567
Run #16

Figure 13 (continued). Examples of Non-buoyant Jets

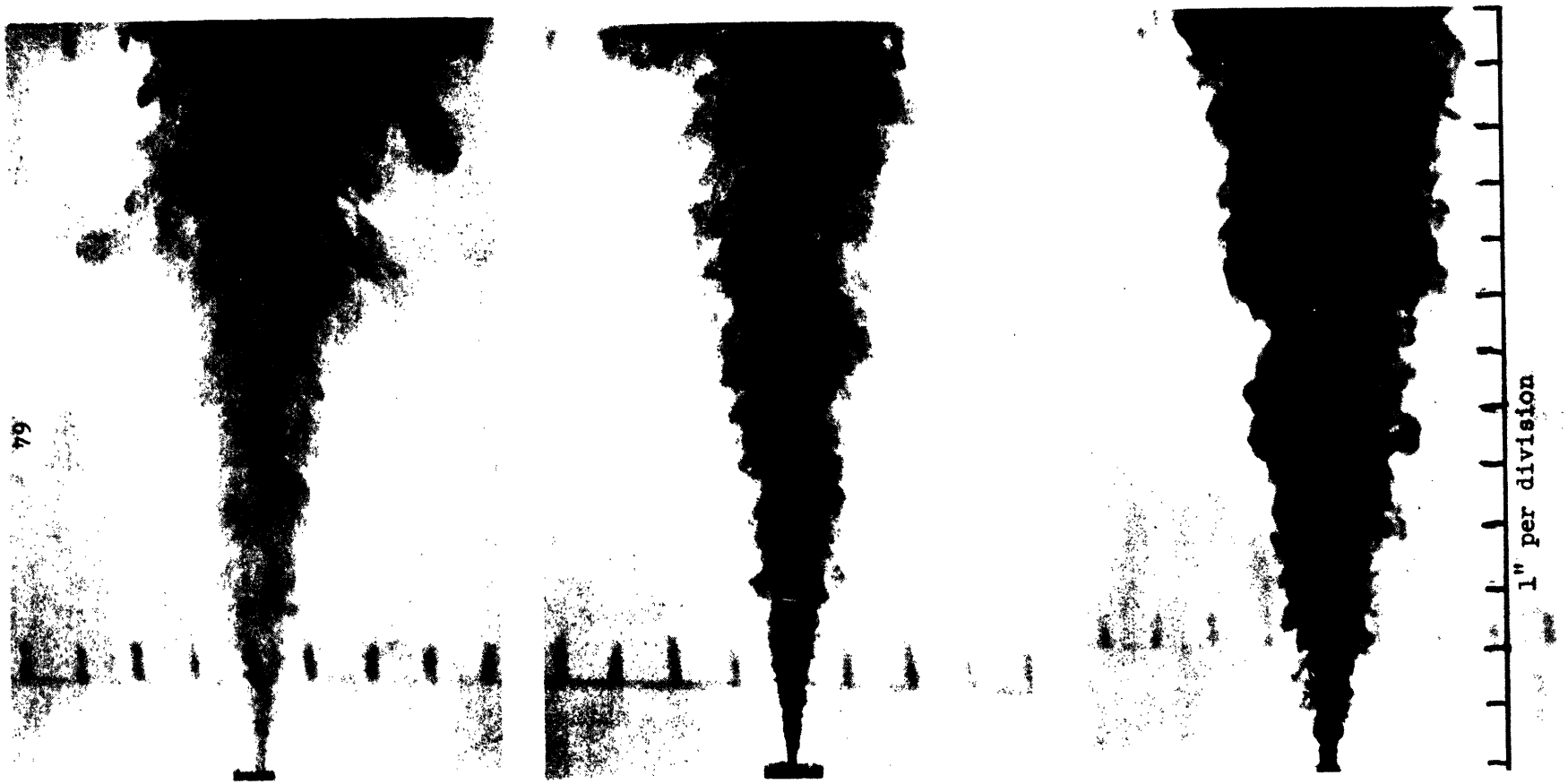

Re = 3608
Run # 2

Re = 4538
Run #30

Re = 9857
Run # 7

Figure 13 (continued). Examples of Non-buoyant Jets

C. Buoyant Jets

Tables 6 and 7 show the results of Froude numbers 10 and 25 for jets affected by buoyancy. A pattern of results similar to those of the non-buoyant jet is shown. Runs of Reynolds number below 1000-1200 have a larger exponent in Equation 26 than those above Re = 1000-1200. A few runs below Re = 1200 have low correlation coefficients, indicating a change in slope caused by a laminar length breaking down to turbulence. Figure 14 plots S_c versus Re for z/d_o = 15 and shows an increase in dilution due to the effect of buoyancy. For Reynolds numbers below 1200-1500, the experimental results show lower values than Abraham's results.

Figure 15 shows S_c^* plotted versus Reynolds number for F = 25 and 10. These experiments show general agreement with values of S_c^* found in Table 3. The generally higher values of S_c^* for buoyant jets over non-buoyant jets is confirmed by these results and shows that dilution increases more rapidly for lower Froude numbers than for higher Froude numbers for Re > 1200.

Figure 16 shows S_V^* plotted versus Re for F = 25 and 10 and λ^2 = 2. Values of S_V^*/S_c^* shown in Tables 6 and 7 for buoyant jets do not agree as well with the value predicted by Taylor's assumption of $\lambda^2 = 2$. The values of this ratio for a Froude number of 10 support an increased value of λ. Since buoyancy increases the turbulent intensity, the temperature profile would be expected to spread further from the velocity profile than for the non-buoyant

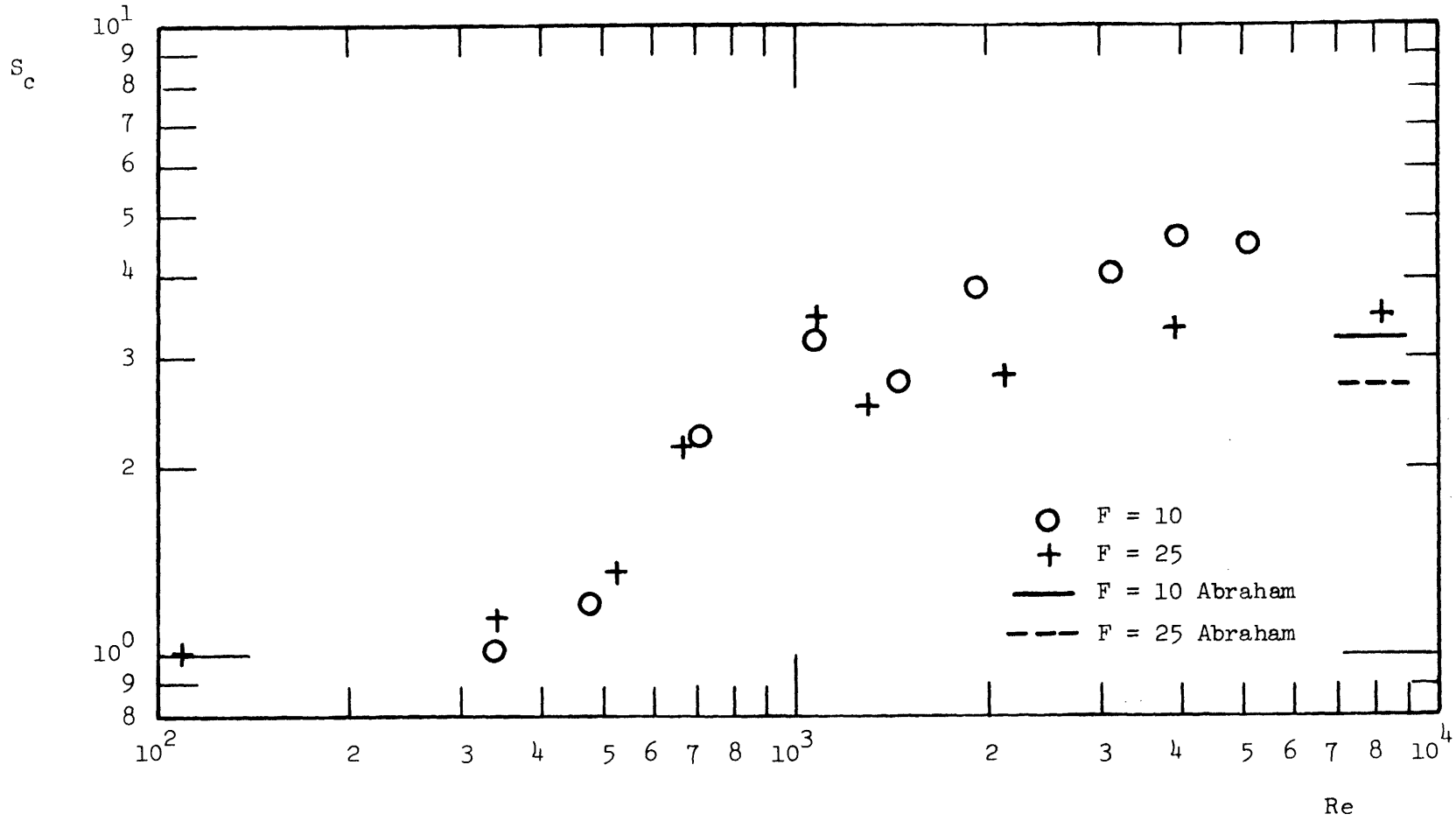

Figure 14. S_c versus Reynolds Number for Buoyant Jets at $z/d_o = 15$

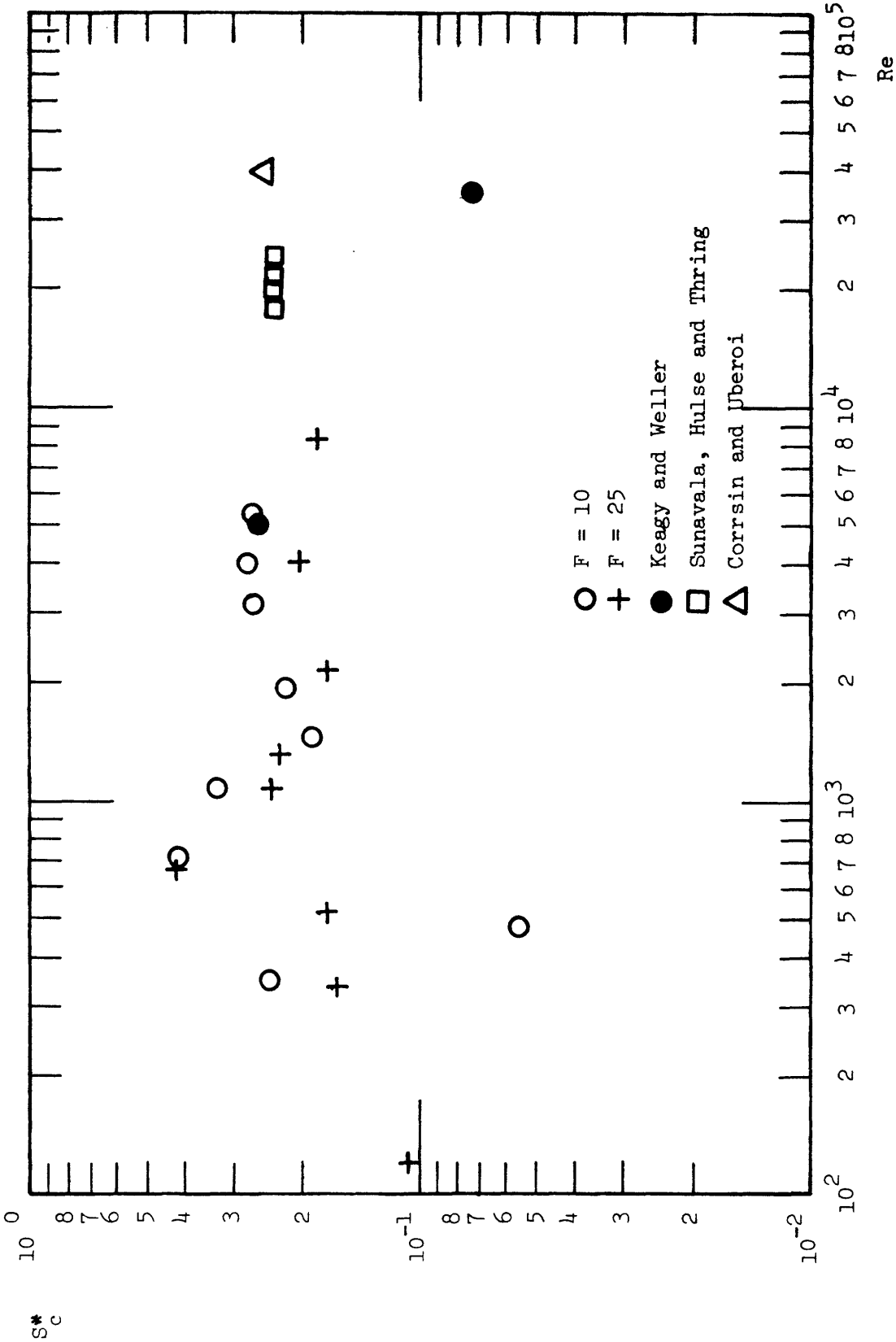

Figure 15. S_c^* versus Reynolds Number for Buoyant Jets

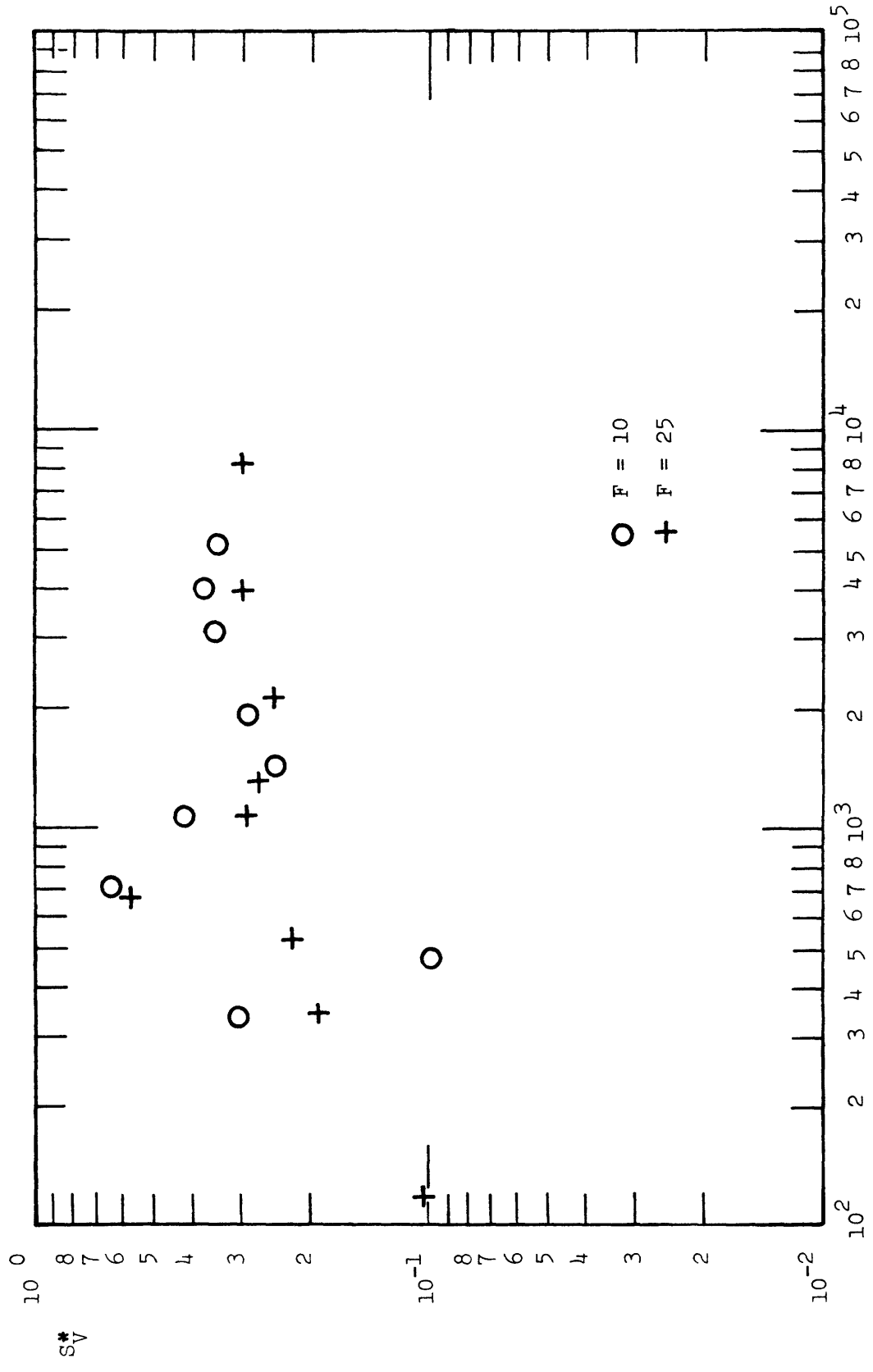

Figure 16. S_V^* versus Reynolds Number for Buoyant Jets ($\lambda^2 = 2$)

case.

Figure 16 shows a similar behavior of the coefficient S_V^* versus Re as Figure 15 shows for S_c^* versus Re. The rate of dilution increase is fairly constant for Re > 1200; below 1200 the data of Figures 15 and 16 rise to a peak, and after Re = 700, fall off rapidly. This pattern of variation is similar in form to the familiar Reynolds number effect on other physical quantities, such as drag and friction coefficients. The results shown in Figures 9 and 10 for non-buoyant show a similar pattern, although the fall off below Re = 700 is not as well substantiated. The increase in the rate of dilution for 700 < Re < 1200-1500 is more pronounced for the buoyant jets, and this is probably due to the buoyancy aided breakdown into turbulence which occured for jets in this range. The fact that only a few experiments show increased dilution in this range of Reynolds numbers does not allow any substantive conclusions to be made concerning the effect or probable cause of this dilution rate increase.

Table 9 gives the laminar length and cone angle for the buoyant runs. These are plotted in Figures 17 and 18. The variation of laminar length and cone angle with Reynolds number for buoyant jets differs from those for non-buoyant jets. The laminar length for the buoyant jets is slightly smaller than those for non-buoyant jets, which is to be expected since buoyancy would tend to increase jet instability. Cone angle for Re > 1500-2000 are generally a few

Table 9

LAMINAR LENGTH AND CONE ANGLE FOR BUOYANT JETS

Froude Number = 10						Froude Number = 25					
Run #	Froude #	Reynolds #	Diameter (inches)	Laminar Length z_1/d_o	Cone Angle $2\alpha_t^o$	Run #	Froude #	Reynolds #	Diameter (inches)	Laminar Length z_1/d_o	Cone Angle $2\alpha_t^o$
14	8.1	338	0.1875	11.3	18°	27	32.9	109	0.125	>50.0	--
28	10.5	475	0.1875	22.7	22°	25	28.8	342	0.125	32.0	27°
33	10.4	712	0.25	4.0	19°	26	20.9	519	0.125	13.0	17°
34	10.0	1080	0.25	2.0	18°	17	24.1	662	0.125	8.0	20°
5	8.8	1447	0.375	0	25°	29	26.1	1079	0.1875	2.0	20°
9	9.9	1934	0.5	0	21°	15	24.2	1304	0.1875	4.0	21°
31	10.1	3150	0.5	0	24°	1	27.2	2124	0.25	1.0	23°
11	10.0	4013	0.75	0	22°	6	24.3	3967	0.375	0	21°
12	8.9	5151	0.75	0	23°	10	23.9	8228	0.5	0	23°

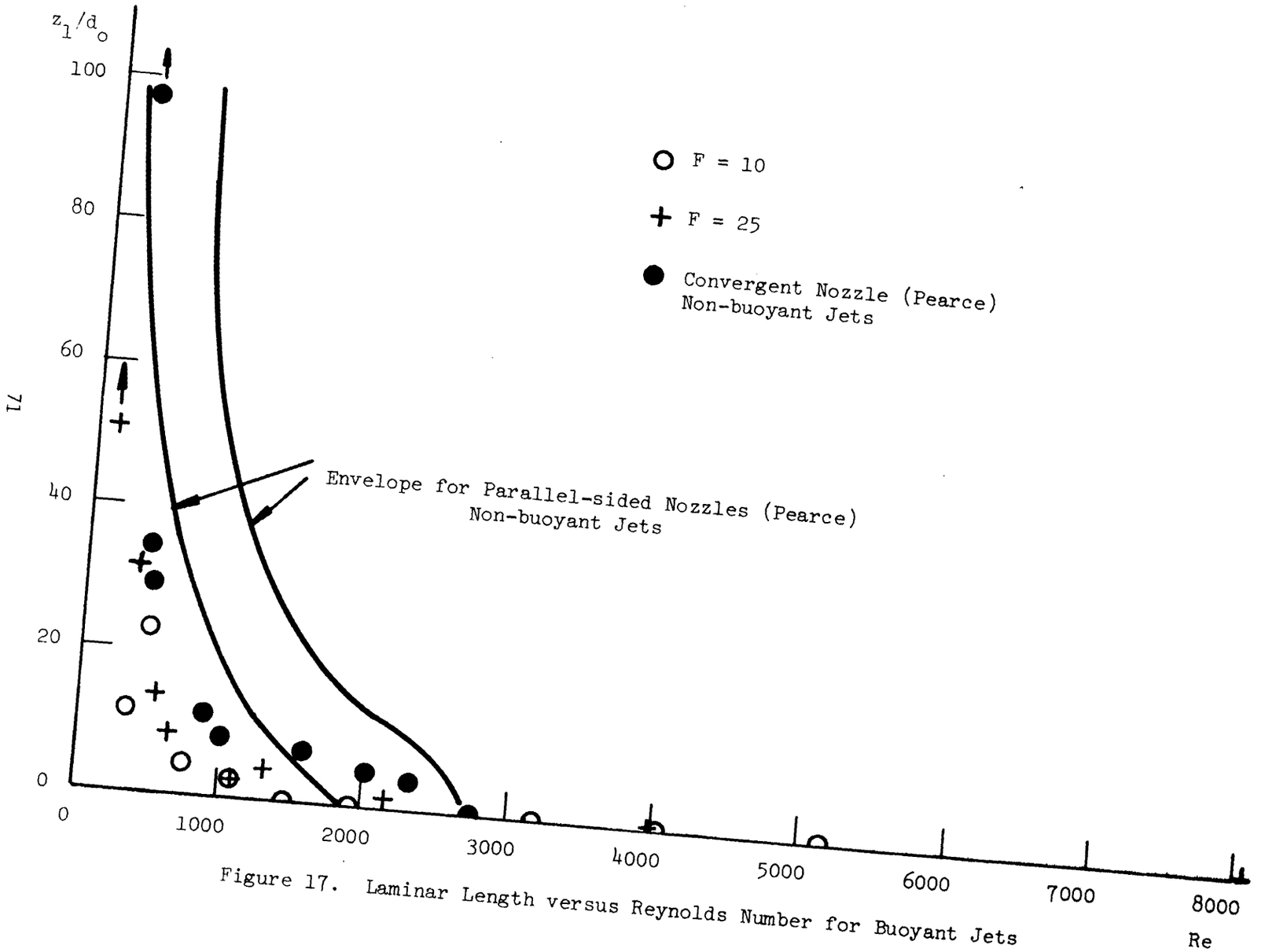

Figure 17. Laminar Length versus Reynolds Number for Buoyant Jets

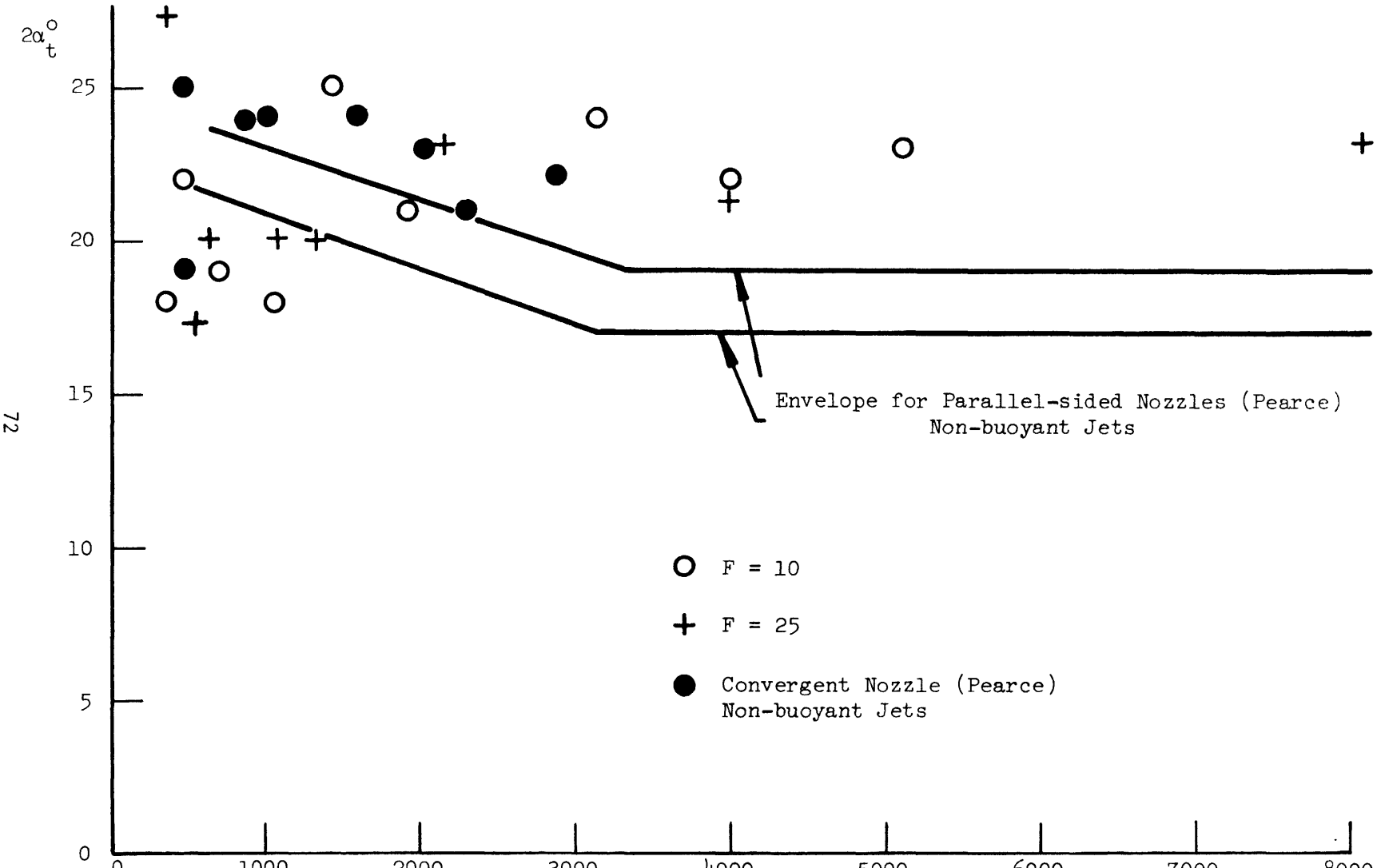

Figure 18. Cone Angle versus Reynolds Number for Buoyant Jets

degrees larger for buoyant jets over non-buoyant jets, which supports the increased value of λ for buoyancy aided turbulence discussed earlier. As the Reynolds number decreases below Re = 1500, the cone angle generally decreases for buoyant jets. Experimental results for plume-like behavior show a lower value of λ for the thermal plume than for the turbulent jet. Thus the results showing a decrease in cone angle for lower Reynolds numbers seem reasonable because of a lower level of turbulence.

Figure 19 shows photographs of experiments for buoyant jets. The horizontal, dotted line on each picture indicates the extent of the inertial, non-buoyant range as predicted by Abraham (1). Changes in cone angle and laminar length can be noticed for these buoyant jets compared to the non-buoyant jets of Figure 13.

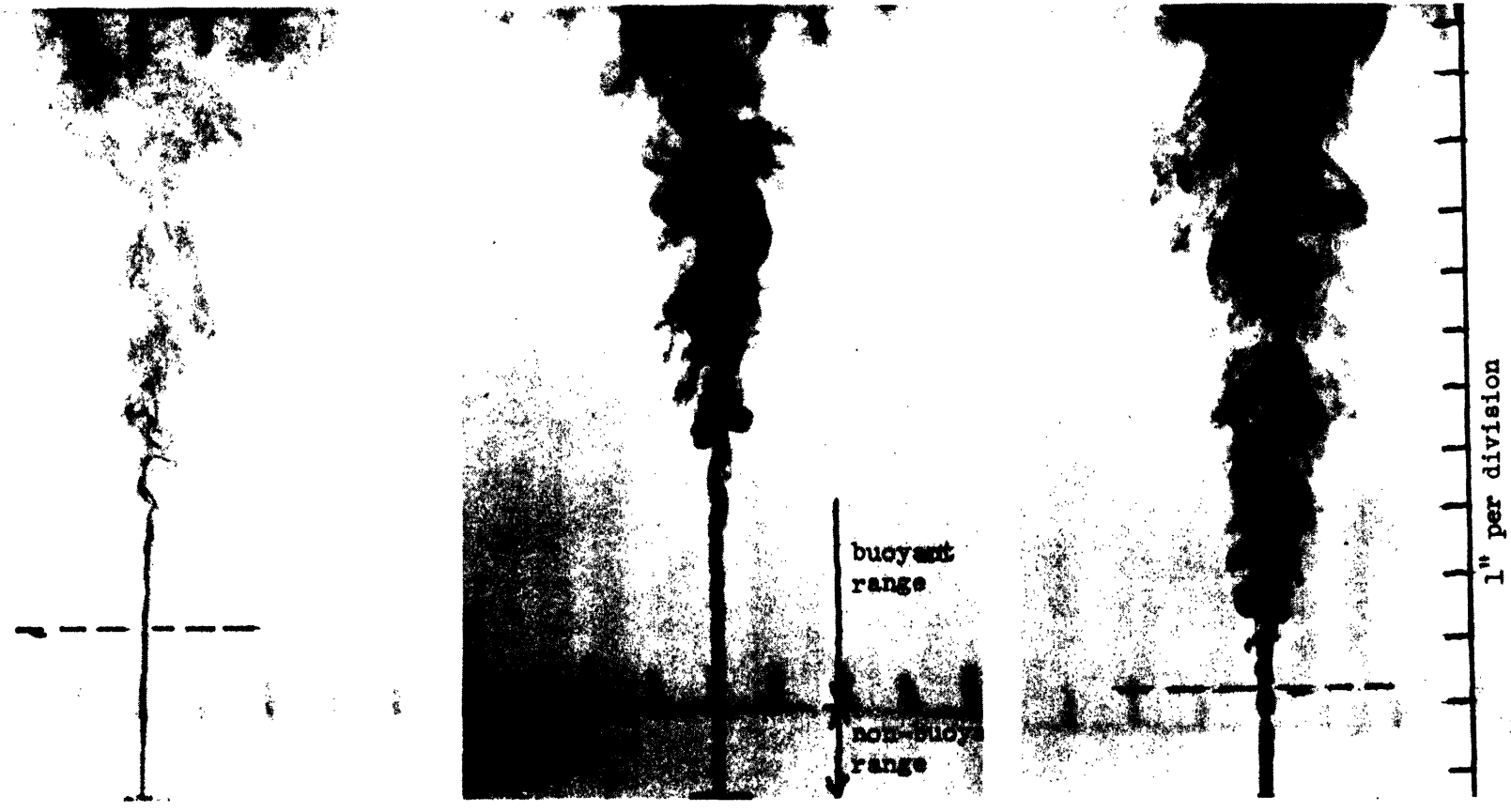

Re = 342
Run #25

Re = 475
Run #28

Re = 712
Run #33

Figure 19. Examples of Buoyant Jets

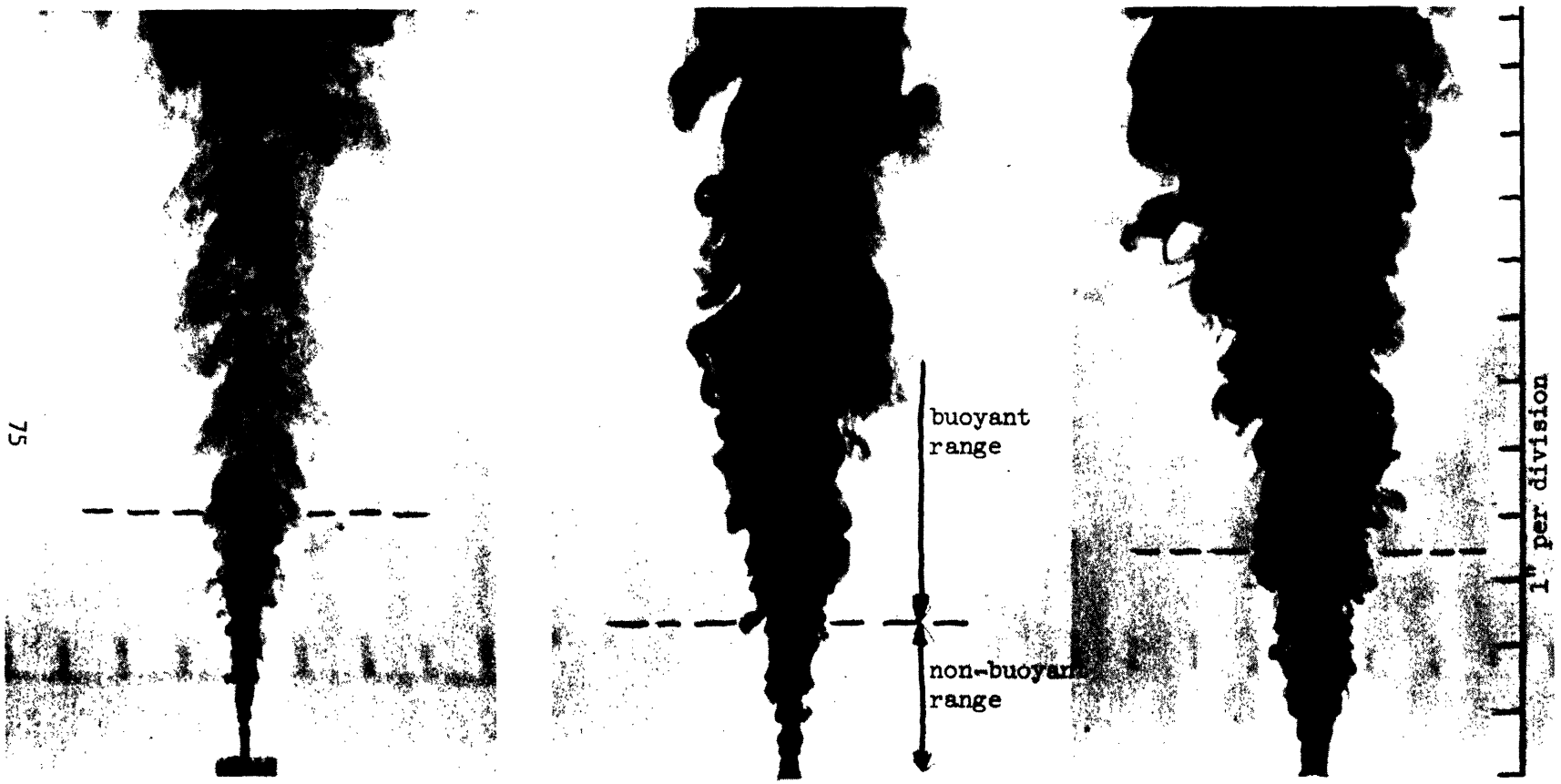

Re = 1079
Run #29

Re = 1447
Run # 5

Re = 1934
Run # 9

Figure 19 (continued). Examples of Buoyant Jets

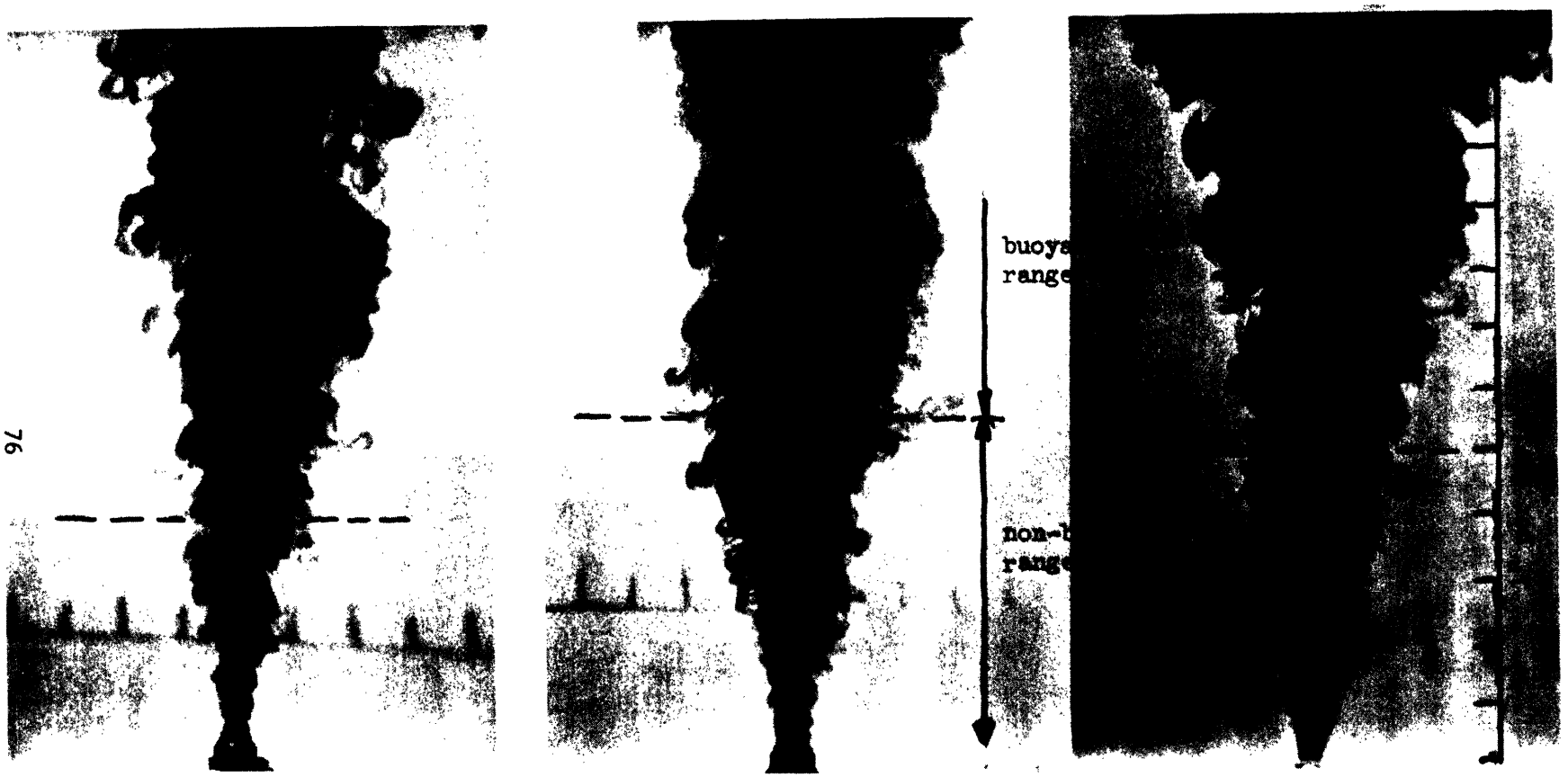

Re = 3150
Run #31

Re = 4013
Run #11

Re = 8228
Run #10

Figure 19 (continued). Examples of Buoyant Jets

VII. Conclusions

A. Non-buoyant Jets

1. Turbulent jet dilution occurs for Reynolds numbers greater than 1500. The structural properties noted by Pearce (18) are generally supported, but direct measurement of dilution reveals that a predominantly turbulent jet, defined as a jet whose laminar length does not exceed the length of a turbulent jet's potential core, has turbulent jet dilution capability.

2. Modeling of turbulent jets is acceptable for Re > 1500, provided no other physical constraint becomes binding and provided the jet's laminar length does not become significantly large compared to the maximum distance available for entrainment along the path of the jet axis. This maximum distance is defined as the distance along the path of the jet axis from the nozzle to a physical boundary, such as a solid obstacle, an ambient layer of significantly different density, or the free surface.

B. Buoyant Jets

1. Turbulent dilution occurs for predominantly turbulent jets whose Reynolds numbers are greater than 1200 and whose Froude numbers are in the range from 10 to 25. The definition of a predominantly turbulent jet used for non-buoyant jets also applies here. Since greater buoyancy increases the level of turbulent intensity, jets with even lower Froude numbers than those encountered in this study may have an even lower critical Reynolds number. This,

however, is only implied by these results.

The evidence presented here supports a slightly different description of jet characteristics in the laminar-turbulent transition for buoyant jets than for the non-buoyant jets described by Pearce. For buoyant jets, the cone angle increases with increasing jet Reynolds number until about Re = 2000, when it becomes constant at a value larger than the cone angle of a turbulent, non-buoyant jet. The laminar length decreases with increasing jet Reynolds number until it disappears at Re = 2000-2500. The laminar length of a buoyant jet is less than the corresponding length in a non-buoyant jet. The instability of a buoyant jet occurs at a lower Reynolds number than the non-buoyant jet. The only laminar buoyant jet investigated in this study had a Reynolds number of 100, while buoyant jets for Reynolds numbers greater than 340 became unstable at some distance and broke down to turbulence.

2. Modeling of buoyant jets of Froude numbers 25 and 10 is acceptable for Re > 1200, provided the constraints on the laminar length mentioned in the conclusions for non-buoyant jets do not become binding.

VIII. Future Work

There always exists the alternative of improving the experimental equipment and apparatus used in any experimental study. Improvements in the equipment used in this study might include refined flow measurement and temperature regulation by mixing hot and cold water in a large mixing chamber to the correct temperature, before issuing the water through the jet. This would help damp temperature oscillations and help remove air bubbles entirely. A means of obtaining temperature profiles in a form that is easily available to a computer rather than using graphs would simplify data reduction.

With respect to the results for non-buoyant jets, more experiments are needed to substantiate nearly laminar Reynolds number behavior as well as the range $700 > Re > 1200$ where there is some evidence of an increased dilution rate. A useful strategy which was not discovered in time for use in this study is to make use of ambient water temperature below 40°F commonly occuring during the months of January and February at the Ralph M. Parsons Laboratory. Because of the nearly constant density of water below 50°F, a fairly low density difference between the jet and ambient water can be obtained with a relatively high temperature difference for measurement purposes. Thus, very high Froude number jets over the entire range of transition Reynolds numbers can be studied.

With respect to buoyant jets, further study is needed to

investigate Reynolds number effects over a greater range of low densimetric Froude numbers. The range of increasing rate of dilution for $700 < Re < 1200$ needs further study.

IX References

1. Abraham, G., "Jet Diffusion in Liquid of Greater Density", Proceedings of the American Society of Civil Engineers, Journal of the Hydraulics Division, Volume 86, HY6, June, 1960, pp. 1-13.

2. Abraham, G., "Jet Diffusion in Stagnant Ambient Fluid", Delft Hydraulics Laboratory, Publication #29, July, 1963.

3. Abramovich, G.N., The Theory of Turbulent Jets, Cambridge, Massachusetts, M.I.T. Press, 1963.

4. Albertson, M.L., Dai, Y.B., Jensen, R.A. and Rouse, H., "Diffusion of Submerged Jets", Transactions, American Society of Civil Engineers, Volume 115, 1950, pp. 639-697.

5. Becker, H.A., Hottel, H.C., and Williams, G.C., "The Nozzle-Fluid Concentration Field of the Round, Turbulent, Free Jets", Journal of Fluid Mechanics, Volume 30, Part 2, 1967, pp. 285-303.

6. Brooks, N.H., "Prediction of Dilution and Submergence for Outfall Diffusers-State of the Art", Lecture Notes, American Society of Civil Engineers Hydraulics Conference, Ithaca, New York, August, 1972.

7. Cleeves, V. and Boelter, L.M.K., "Isothermal and Non-Isothermal Air-jet Investigations", Chemical Engineering Progress, Volume 43, No. 3, March 1947, pp. 123-134.

8. Corrsin, S. and Uberoi, M.S., "Further Experiments on the Flow and Heat Transfer in a Heated Turbulent Air Jet", National Advisory Committee for Aeronautics, Technical Note 1865, April 1949.

9. Daily, J.W. and Harleman, D.R.F., Fluid Dynamics, Reading, Massachusetts: Addison-Wesley Publishing Company, Incorporated, 1966.

10. Fan, L. and Brooks, N.H., "Numerical Solutions of Turbulent Buoyant Jet Problems", W.M. Keck Laboratory of Hydraulics and Water Resources, Report #KH-R-18, Pasadena, California, January 1969.

11. Forstall, W. and Gaylord, E.W., "Momentum and Mass Transfer in a Submerged Water Jet", American Society of Mechanical Engineers, Journal of Applied Mechanics, Volume 22, #2, June 1955, pp. 161-164.

12. Hinze, J.O., Turbulence, New York: McGraw-Hill Series in Mechanical Engineering, 1959.

13. Hinze, J.O. and van der Hegge Zijnen, B.G., "Heat and Mass Transfer in the Turbulent Mixing Zone of an Axially Symmetrical Jet", Seventh International Congress for Applied Mechanics, 2, Part 1, 1948, pp. 286-299.

14. Jirka, G. and Harleman, D.R.F., "The Mechanics of Submerged Multiport Diffusers for Buoyant Discharges in Shallow Water", Ralph M. Parsons Laboratory for Water Resources and Hydrodynamics, Report #169, March 1973.

15. Jirka, G., Koester, G. and Harleman, D.R.F., "Experimental Study of a Submerged Multiport Diffuser in a Tidal Bay (Condenser Water Discharge from the Main Yankee Atomic Power Station)", Ralph M. Parsons Laboratory for Water Resources and Hydrodynamics, Report #184, April 1974.

16. Keagy, W.R. and Weller, A.E., "A Study of Freely Expanding Inhomogeneous Jets", Proceedings, Heat Transfer and Fluid Mechanics Institute, Palo Alto, California, 1949, pp. 89-98.

17. Mollendorf, J.C. and Gebhart, B., "An Experimental and Numerical Study of the Viscous Stability of a Round Laminar Vertical Jet with and without Thermal Buoyancy for Symmetric and Asymmetric Disturbances", Journal of Fluid Mechanics, Volume 61, Part 2, 1973, pp. 367-399.

18. Pearce, A.F., "Critical Reynolds Number for Fully-Developed Turbulence in Circular Submerged Water Jets", Council for Scientific and Industrial Research, Report MEG 475, Pretoria, South Africa, August 1966.

19. Ricou, F.P. and Spalding, D.B., "Measurements of Entrainment by Axisymmetrical Turbulent Jets", Journal of Fluid Dynamics, Volume 11, Part 1, 1961, pp. 21-32.

20. Ruden, P., "Turbulent Ausbreitungsvorgange im Freistrahl", Die Naturwissenschaften, Jahrg. 21, Heft 21/32, May 26, 1933, pp. 375-378.

21. Schlichting, H., Boundary Layer Theory, Sixth Edition, New York: McGraw-Hill Book Company, 1968.

22. Sunavala, P.D., Ph.D. thesis, University of Sheffield, England.

23 Sunavala, P.D., Hulse, C. and Thring, M.W., "Mixing and Combustion in Free and Enclosed Turbulent Jet Diffusion Flames", Combustion and Flame, Volume 1, 1957, pp. 179-193.